2013

Interaction Between Maltose Binding Protein And Escherichia Coli Maltose Transporter

Yan Huang
Purdue University, yanhuang.eco@gmail.com

Graduate School ETD Form 9
(Revised 12/07)

PURDUE UNIVERSITY
GRADUATE SCHOOL
Thesis/Dissertation Acceptance

This is to certify that the thesis/dissertation prepared

By Yan Huang

Entitled
INTERACTION BETWEEN MALTOSE BINDING PROTEIN AND ESCHERICHIA COLI MALTOSE TRANSPORTER

For the degree of Master of Science

Is approved by the final examining committee:

Jue Chen
Chair

David M. Umulis

Frederick S. Gimble

Christine A. Hrycyna

Cynthia V. Stauffacher

To the best of my knowledge and as understood by the student in the *Research Integrity and Copyright Disclaimer (Graduate School Form 20)*, this thesis/dissertation adheres to the provisions of Purdue University's "Policy on Integrity in Research" and the use of copyrighted material.

Approved by Major Professor(s): Jue Chen

Approved by: Christine A. Hrycyna 11/07/2013
Head of the Graduate Program Date

INTERACTION BETWEEN MALTOSE BINDING PROTEIN AND *ESCHERICHIA COLI* MALTOSE TRANSPORTER

A Thesis

Submitted to the Faculty

of

Purdue University

by

Yan Huang

In Partial Fulfillment of the

Requirements for the Degree

of

Master of Science

December 2013

Purdue University

West Lafayette, Indiana

谨此献给我的父亲，母亲，爱人和恩师。

For my father, mother, my love, and Amy.

ACKNOWLEDGEMENTS

I am sincerely grateful to my advisor, Dr. Amy L. Davidson, who lost her battle against cancer in April 2013. She guided me to explore the mystery of maltose transporter with her profound knowledge and insightful opinions. Her intelligence and enthusiasm for her work motivated me to pursue science. Her kindness and humble personality warmed my heart.

I thank my current advisor Dr. David Umulis for fully supporting me to complete my previous work and continue my PhD studies. I thank Dr. Jue Chen, who helped me through the most difficult period. Without her support and guidance, I wouldn't have finished my master thesis project, or made the smooth transition to my PhD study. I am grateful to Dr. Frederick S. Gimble who keeps encouraging me even when Dr. Davidson was weak. I thank my two other committee members, Dr. Cynthia Stauffacher and Dr. Christine A. Hrycyna, for their time, expertise and suggestions.

I thank Dr. Candice Klug, Dr. Mike Everly, Dr. Lake Paul, and Dr. Alexander Wei for lending their expertise in collaborative projects with the Davidson lab. I thank Emily Bramson and Karen Sue Malady for their patience and organization skills as they processed my documents and plans of study.

I thank Frances J. Alvarez, Shanshuang Chen, Shiming Huang, Michael Oldham, Cedric Orelle and Austin Rice for offering suggestions regarding scientific thinking,

troubleshooting, and even personal life. I thank members of Dr. Jue Chen's group: Alanna Steffen-Nelson, David Yin-wei Lin, Mi Sun Jin, Sara Qiuju Zhang, Xiaoxiao Li, Wei Mi, Shuo Huang and Carol J. Greski. I thank everyone who has been a member of the Davidson laboratory and all the group members of the Umulis laboratory.

I thank all my dear friends. Special thanks go to Dr. Jue Chen, Margaret Kalcic, Ankush Charkrabarty, Shanshuang Chen, Kaibo Zhang, Yafang Chen, Fei Han and Yao Wang for commenting on my thesis.

Last but not least, I thank my family. I thank my grandparents and my aunts for believing in me. I thank my parents and Hang Yu for everything.

TABLE OF CONTENTS

Page

Page

LIST OF TABLES

LIST OF FIGURES

ABSTRACT

Huang, Yan. M.S., Purdue University, December 2013. Interaction between Maltose Binding Protein and *Escherichia Coli* Maltose Transporter. Major Professor: Amy L. Davidson (late) and Jue Chen.

The ATP-binding cassette (ABC) transporter superfamily is one of the largest families of transport proteins. The ABC transporters are responsible for selective permeability of solute across membranes energized by ATP hydrolysis, which occurs in all domains of life. Maltose transporter is an ABC importer that mediates maltose/maltodextrin uptake in bacteria and archaea. It is identified as an essential virulence factor in pathogenic species of *Streptococcis pyogenes* and *Vibrio cholera* (*1, 2*). *Escherichia coli* maltose transporter is a well-characterized system with crystal structures and exclusive biochemical studies available. Knowledge of the *E. coli* maltose transport mechanism will lead to a better understanding of maltose transporters in the other species as well as other classes of ABC importers.

The goal of this study was to characterize the mechanism by which the substrate binding protein stimulates the transport cycle. To study how MBP initiates the transport process, MBP was spin-labeled at a single residue of the N-lobe and the mobility surrounding the labeling site was detected by Electron Paramagnetic Resonance. The

second periplasmic loop of MalF, P2, was found to bind with MBP N-lobe throughout the catalytic cycle, suggesting that P2 is involved in the recruitment of MBP, as corroborated by previous studies. In addition, a lack of mobility change at the interface of the MBP N-lobe and P2 suggested that the 5 Å decrease in the distance between MBP and MalF-P2 upon addition of ATP or maltose from previous crosslink study is likely due to a rotation between MBP and P2. In comparison, maltose decreased the mobility between MalG P3 and MBP at residue 41, suggesting that P3s' conformation may be sensitive to maltose binding.

Among the periplasmic loops of the transmembrane domains, the MalF-P2 loop shares an extraordinarily large interface with MBP N-lobe. It is possible that P2 has essential roles other than recruiting MBP. However, this is questioned by the fact that P2 is missing in gram-positive and archaea maltose transporters. To test the functional roles of this region, P2 was truncated and the maltose transporter mutant without P2 was tested through *in vivo* maltose transport assays and then *in vitro* ATPase activity assay in nanodiscs. Results demonstrate that the interaction between P2 and MBP is essential to maltose transport. To further investigate the functions of P2, a P2-truncated mutant of a binding-protein independent mutant (F500) was constructed. The MacConkey assay result shows that this mutant can transport maltose *in vivo,* indicating that P2 is likely to be involved only in recruiting MBP.

CHAPTER 1. INTRODUCTION: STRUCTURE, FUNCTION AND DYNAMICS OF THE MALTOSE TRANSPORTER IN *ESCHERICHIA COLI*

1.1 ATP-Bing Cassette (ABC) Systems

The ATP-binding cassette (ABC) systems couple the energy of ATP hydrolysis to import and export molecules, as well as several non-transport-related processes including translation, elongation and DNA repair (*3*). Despite the diverse population of substrates and the difference in the direction of transport, ABC proteins share a common organization composed of two integral membrane domains and two peripheral ABC domains (*4*). The sequence and structure of the nucleotide-binding domain are highly-conserved. ABC transporters play a significant role in both basic membrane biology and medical applications. In bacteria, ABC transporters are critical for survival; these proteins are targets for the development of antibacterial vaccines and therapies (*5*). In humans, several genetic defects in these proteins play a role in many diseases, such as cystic fibrosis, hyperinsulinemia, and macular degeneration (*4*).

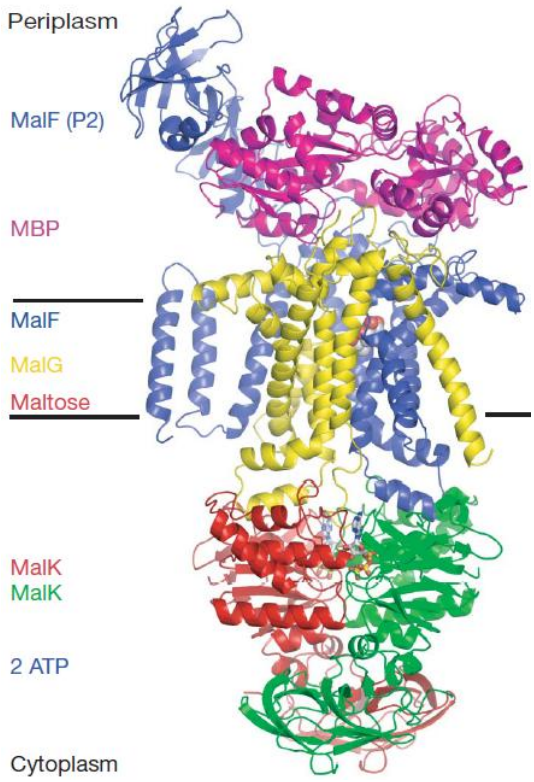

Figure 1.1 Structure of maltose transporter in a catalytic intermediate conformation. PBID is 3PV0 (*6*). Subunits are colored as indicated in the figure.

1.2 Structure of the MBP-MalFGK2 Complex in *E. coli*

E. coli maltose transporter is one of the most extensively-studied among all the ABC transporter systems. A pictorial representation of this system is given in Figure 1.1. The transmembrane domain (TMD) contains an intertwined heterodimer of MalF and MalG. Functional reconstitution of the subunits of *E. coli* maltose uptake system *in vitro*, the $MalFGK_2$ complex, has been demonstrated successfully (*7, 8*). MalG of the *E. coli* maltose transporter is homologous to other species. The N-terminal periplasmic loop of MalF, the P2 loop, is large (approximately 180 residues), but, interestingly, it is unique to Enterobacteriaceae (*9, 10*). Although MalF TM 1 and TM 2 are usually missing in gram-positive or archaea maltose transporters, they can be truncated without affecting

$MalFGK_2$ structure or function (*11*). However, it is unclear whether truncation of P2 will affect the function of *E. coli* maltose transporter. Both MalF and MalG contain three periplasmic loops interacting with MBP and an EAA loop binding tightly with MalK (*6*). MBP is a periplasmic protein in *E. coli* but is usually a lipoprotein anchored to the membrane in gram-positive and archaea maltose transporter systems (*9, 12*).

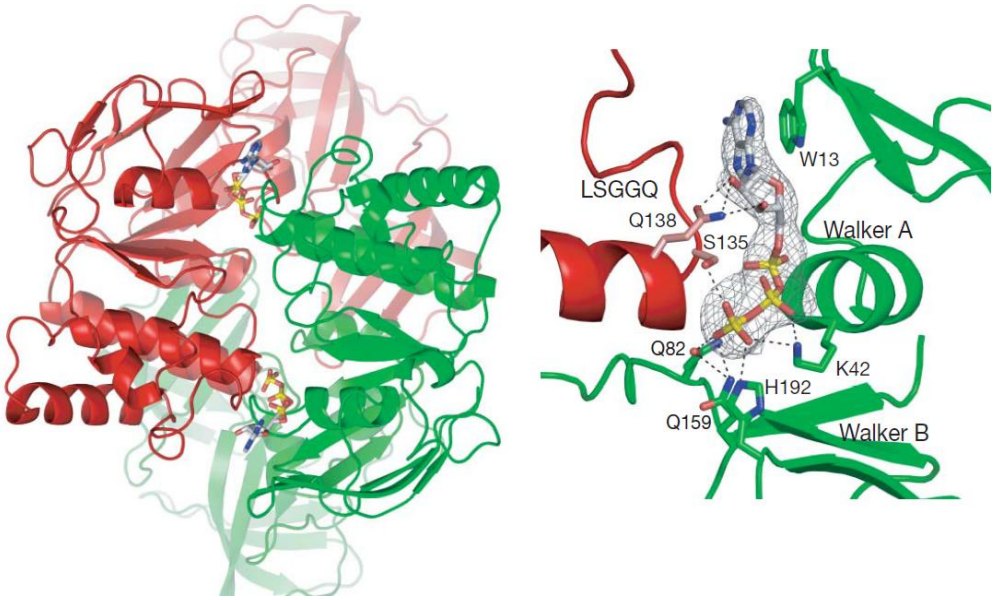

Figure 1.2 Structure of ATP-bound MalK Subunits (*6*). Left, the MalK dimer viewed down the local twofold axis. Right, the ATP-binding site, showing that Walker A and Walker B from one MalK subunit (green) and LSGGQ from the other MalK subunit (red) are making contact with one ATP molecule. ATP is represented in the ball-and-stick model.

Similar to other ABC systems, the N-terminal domain of MalK contains a RecA-like subdomain and a helical subdomain (Figure 1.2). The helical subdomain contains the LSGGQ motif, which is unique to ABC transporters. Like other bacterial ATP-binding cassettes MalK also has a C-terminal regulatory domain. This domain contributes substantially to maintaining two isolated MalK subunits as a dimer even in the absence of

ATP (*13, 14*), whereas other isolated cassettes behave as monomers without ATP. In the crystal structure (*6*), two ATP molecules are bound along the dimer interface contacting residues in the Walker A and B motifs of one MalK monomer and the LSGGQ motif of the other MalK monomer.

The opening and closing motions of the MalK nucleotide-binding interface during ATP hydrolysis drive maltose across the membrane. Interestingly, these motions are demonstrated to be coupled to conformational changes of MBP and MalFG during the translocation cycle (*15-18*). The rate of maltose transport displays a sigmoidal dependence on the MBP concentration, with the half maximal uptake rate at about 25 to 100 μM MBP (*15, 16*). In addition, ATPase activity of the $MalFGK_2$ complex is strongly inhibited by vanadate; however, the isolated MalK is not (*17, 18*). The current progress in studying the coupling of maltose transport and ATP hydrolysis in the catalytic pathway will be introduced in the next section.

1.3 Alternating Access Mechanism of the Maltose Transporter

Three states of the catalytic cycle have been crystallized (*6, 19, 20*): (i) resting state, (ii) pretranslocation (pre-T) state and (iii) transition state (Figure 1.3). In the resting state (Figure 1.3A-B), MalK dimer interface is open and MalFG is facing inward to the cytoplasm (*17, 21, 22*). MalF P2 loop initially interacts with the N-lobe of MBP and assists MBP docking onto MalG. Upon the binding of maltose, MBP is stabilized in the closed conformation.

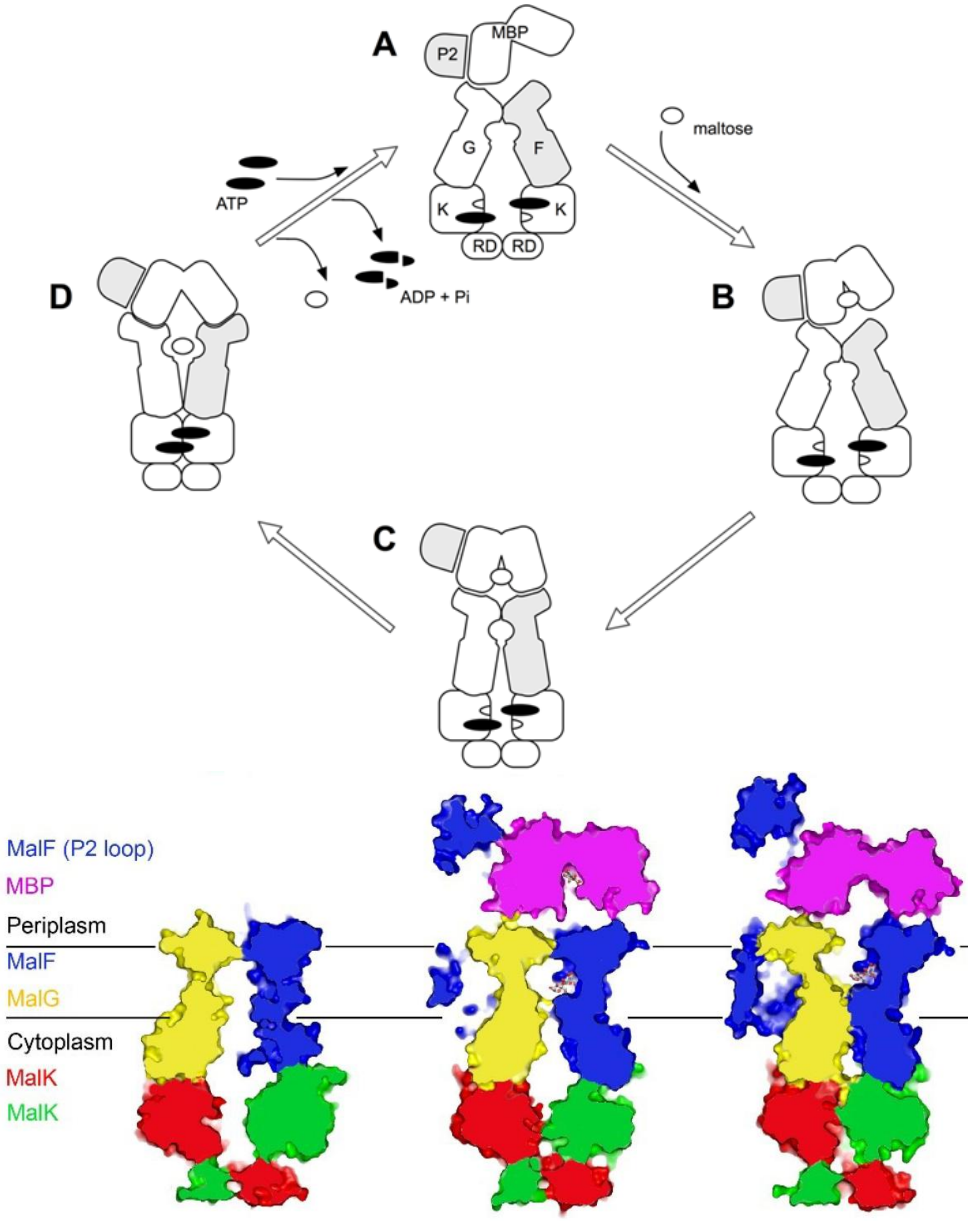

Figure 1.3 Alternating access mechanism of the maltose transporter (*19*, *23*, *24*). (A, B) Resting state: MalK interface is open, MalFG is facing inward and MBP is stabilized in the closed conformation after binding maltose. (C) Pre-T state: MalK interface is semi-open, MalFG is in an intermediate conformation between inward- and outward- facing, and MBP is binding tightly with MalFG. (D) Transition state: MalK interface is closed, MalFG is facing outward and MBP is open, and maltose is translocated to the binding site of MalFG. (D-A) After ATP hydrolysis, the MalK dimer interface opens and MalFG is reoriented to the inward-facing conformation, releasing maltose into the cell. The lower panel shows slab views of the maltose transporter in resting state (left), pre-T state (middle) and transition state (right), respectively.

In the pre-T state (Figure 1.3B-D), the MalK dimer interface is semi-open, MalFG is in an intermediate conformation between inward- and outward- facing, and maltose-bound MBP has a tight binding with MalFG. In the absence of MBP, the resting state transporter displays little ATPase activity, indicating that there is a high energy barrier in the progression from inward- to outward-facing conformations that ATP binding alone cannot overcome (*3, 22, 25*). An intermediate conformation of $MalFGK_2$ was captured by the "pre-T" crystal structure. This intermediate conformation is supposed to be of high-energy since the partial closure of the MalK dimer interface can promote to a fully closed transition state by the addition of Mg ion and the non-hydrolysable ATP analog AMP-PNP (*19, 25*). The detailed mechanism of how the transporter converts from resting state to pre-T is not yet clear. MBP or nucleotide alone does not trigger the conformational changes from resting state to transition state (*3, 22*). The pre-T crystal structure reveals that $MalFGK_2$ can convert to the pre-T state with maltose and MBP in the absence of ATP, and can proceed to the transition state by the addition of Mg ion and the nonhydrolysable ATP analog, AMP-PNP. However, the EPR studies showed no mobility changes for the four single spin mutations labeled at Q-loop (S83C), or the helical subdomain (V120C, Q122C, and A124C) of MalK in the intact transporter following the addition of either maltose-bound MBP or Mg-AMP-PNP alone(*22*). The EPR data are not necessarily inconsistent with the crystal structure since it only indicates no binding or opening at the dimer interface but may not show rotation motions of the MalK dimers. It is likely that MalK dimers rotate toward a partial closure in the presence of maltose-bound MBP without ATP.

In the transition state (Figure 1.3D), the MalK dimer interface is closed and ATP(s) is positioned at the catalytic site for hydrolysis. MalFG turns out-ward facing while MBP is open, allowing maltose to translocate into the low-affinity binding site in MalFG. Radioactive elution profile of the vanadate trapped complex showed that MBP is tightly bound with MalFG and that maltose is not bound tightly by MBP in the vanadate-trapped species. Consistently, the crystal structure of the transition state showed that the open MBP co-crystallizes with the transporter and maltose locates at the MalFG binding site (*6, 19*). The crystal structure of $MalFGK_2$ with wild-type MBP converts from the pre-T state to the transition state when Mg and AMP-PNP are added. In contrast, the pre-T state $MalFGK_2$ with the crosslinked MBP mutant that is locked in the closed conformation cannot proceed to the transition state by the addition of Mg ion and AMP-PNP (*19*). Therefore, the high affinity of open MBP with $MalFGK_2$ in the vanadate-trapping transition state indicates that open MBP may play a key role in stabilizing the outward facing conformation of MalFG (*6, 19, 26*). Theoretically, unliganded MBP should not convert the open MalK dimer to closed dimer conformation. However, experimental data has shown a weak stimulation of unliganded MBP on ATP hydrolysis. This is likely to be due to a very small population of transporters that engage in high-affinity binding with the open MBP and progress far enough toward the transition-state conformation (*27*).

Although a posthydrolysis state of the entire transporter is yet to be crystallized (Figure 1.3D-A), EPR studies and analysis of the isolated NBD structures suggest that ADP is not sufficient to stabilize the closed dimer conformation (*17, 21, 22*). Thus, MalK dimer interface opens after ATP(s) hydrolysis, and MalFG will be likely to reorient to the

inward-facing conformation, releasing the substrate from the low-affinity TMD binding site into the cell through diffusion (Figure 1.3) (*28*).

The studies on mutations of the transporter comparing the ATPase activities of the intact transporter and those of the isolated MalK dimers provides more detailed information on sites possibly involved in the coupling between MalK and MBP. The stimulatory effect of MBP on the ATPase activity of the intact transporter is prevented by the mutation of residue Q140 following the LSGGQ motif while the ATPase activity of isolated MalK is not affected by MBP, suggesting a role of the LSGGQ motif in the communication between MBP and MalK (*21*). The P2 (second periplasmic) loop of MalF, the first periplasmic (P1) loop of MalG and the EAA loop of MalG were reported by mutation suppressor studies to be involved with the communication between MBP and MalK (*28*). Researchers have sought to unveil the mystery of this coupling between substrate translocation and ATP hydrolysis through isolation and analysis of the binding protein-independent (BPI) mutants of the maltose transporter, as described in the next section.

1.4 Binding Protein-Independent (BPI) Mutants

Binding protein-independent (BPI) transporters can transport maltose into the cell independently of MBP (*29, 30*). A pictorial presentation of BPI in comparison with wild-type maltose transporter is given in Figure 1.4A. BPI mutants are similar to the wild-type in terms of maltose-specificity, as well as the affinity, cooperativity, vanadate sensitivity, and substrate specificity of the ATP binding sites (*25, 30, 31*). Genetic analysis shows that BPI requires two mutations. Usually, one is located at the C-terminus of the

transmembrane helix while the other is located in a periplasmic loop which exposes the maltose binding site of the transmembrane domain to the periplasm and perturbs the productive interaction between MBP and the transporter (*23*).

(A)

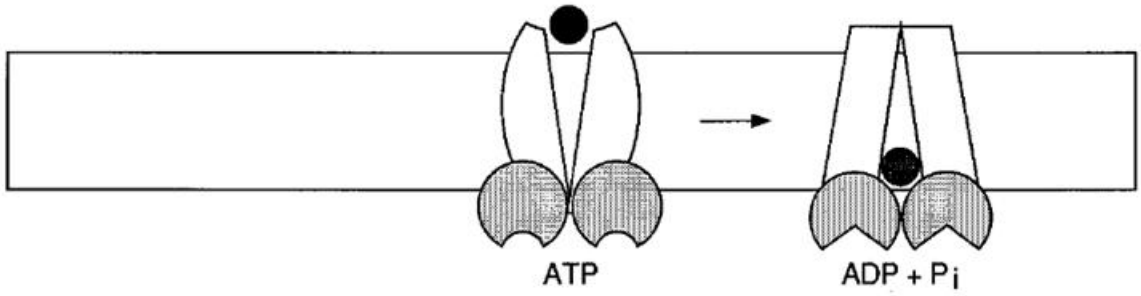

(B)

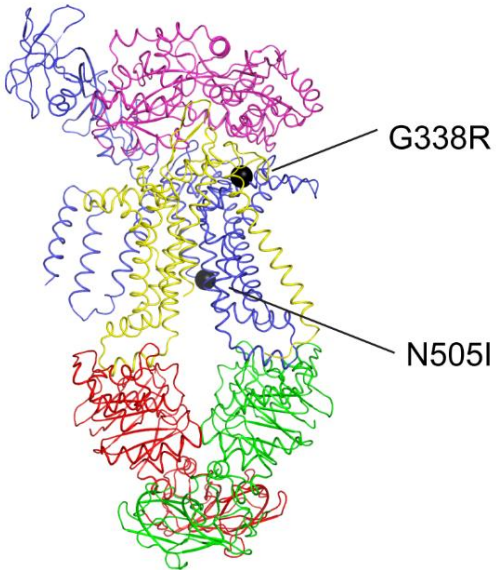

Figure 1.4 A binding protein (BPI) mutant of the maltose transporter. (A) Model for BPI maltose transport (*31*). (B) Structure of the maltose transporter (PBD ID: 3PV0) with sites of the BPI mutation F500 labeled (MalF G338R and N505I). The sphere in red is G338 at MalF. The sphere in grey is N505 at MalF C-terminus. Color codes: purple, MBP; yellow, MalF; cyan, MalG; red and green, MalK dimer.

MBP was found to have an effect on the BPI catalytic cycle different from that of the wild-type transporter. As the concentration of MBP increases, its stimulation on

maltose transport and ATPase activity of the wild-type maltose transporter keep increase and then go flat when MBP concentration is saturated. In contrast, higher concentration of MBP (>1mM) severely inhibits maltose transport of BPI, perhaps because MBP fails to separate from the BPI, or it shifts MalK to an open rather than a closed conformation while bound maltose are not delivered to the membrane binding site (*32, 33*). However, in some BPI mutants such as MalG511 $MalFGK_2$ transporter, MBP at lower concentrations still stimulates maltose transport (*34*). Efforts have been made by researchers on a better understanding of the mechanism of the BPI mutants in order to gain us more knowledge on the mechanism of the wild-type transporter.

Different statements about the resting conformation of BPI can potentially explain the working mechanism of BPI. One explanation is that the transporter rests in an outward-facing state which exposes the low-affinity transmembrane maltose binding site to the periplasm (*35*). This is based on the identical protease susceptibility data of BPI periplasmic loops of MalF and MalG and of the transition-state maltose transporter mutant (MalKE159Q) MalF and MalG (*35*). A more rational explanation is that BPI rests in a high-energy intermediate state which can easily proceed to the transition state in the presence of nucleotide (*19, 25*). Fluorescence data supportive to this explanation showed that the accessibility of the BPI ATP-binding site is less than that of the wild-type transporter at resting state and similar to the wild-type transporter in the presence of MBP and vanadate (*36*).

Based on these findings, we assume that the double mutations of BPI drives the majority of the MalK domains to rest in a semi-open conformation that favors proceeding to closed conformation in the presence of ATP and Mg. MBP is no longer required to

overcome the energy barrier of a shift from open to semi-open conformation. Maltose can also enter the MalFG binding site because the site is exposed to the periplasm. F500 is one of the BPI mutants with mutations of MalF G338R and N505I (Figure 1.4B). F500 was used in this work on the function of P2 by constructing a P2-deleted mutant of F500 as described in Chapter 4.

CHAPTER 2. EXPERIMENTAL PROCEDURES

2.1 Mutagenesis

The Quikchange II XL site-directed mutagenesis kit (Stratagene) was used to generate single mutations in the variants of the *malE* gene encoding MBP with a C-terminal polyhistidine tag (*37*). We constructed the double mutants of malF by two steps of single mutation with the PCR machine and PfuUltra II Fusion HS DNA Polymerase and then digested with DpnI. The sequences of the mutant genes were verified by DNA sequencing. Dr. Michael Oldham replaced 164 residues (94 to 257) of MalF-P2 in the maltose transporter by a short linker of GSGSG, and the mutant is named MalF(ΔP_2)GK_2 (figure 2.1). *In vivo* function of the mutant proteins was confirmed by complementation of a chromosomal deletion of malE, malF, malG, malK (strain AD126 (*argH his rpsL1 malTc, malB*Δ*13* Δ*uncBC ilv::Tn10, F'lacIq Tn5*), as judged on 1 % maltose MacConkey agar (Difco) (*38*). Plasmid-encoded mutants that are functional yield colonies that turn red after incubation overnight at 37 ℃.

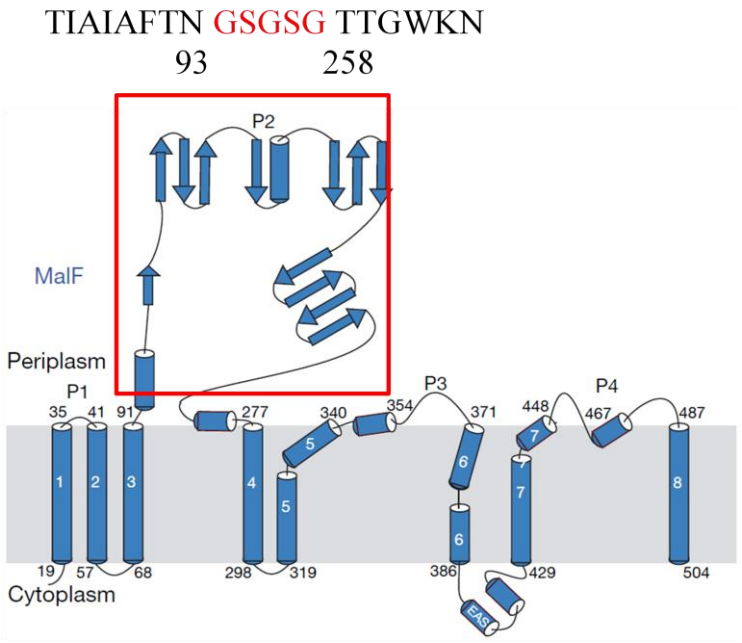

Figure 2.1 Diagram of the secondary structure of MalF (blue) with P2 highlighted in red square. The amino acid residues 94-257 of MalF-P2 are replaced with GSGSG (6).

2.2 *In vivo* maltose transport assay: MacConkey assay

MacConkey plates were prepared by autoclaving MacConkey agar and then supplementing with 1% maltose and antibiotics. *E. coli* strain AD126 carrying a genomic deletion of malE, malF and malG, was transformed with plasmids encoding different combinations of the wild-type or mutant *E. coli* maltose transporter components. The cells of the transformed strains were then spread on MacConkey plates. Colonies were observed after incubations of either 12 hours or 14 hours at 37 ℃. Red and white colonies indicate efficient (positive) and deficient (negative) maltose transport, respectively.

2.3 Expression and Purification of Proteins

2.3.1 Expression and Purification and Assembly of $MalFGK_2$ Complex

MalF, MalG and MalK were overexpressed simultaneous with two plasmids in the strain AD126 (*argH his rpsL1 malT^c malB*Δ*13* Δ*uncBC ilv::Tn10 F'lacI^Q* Tn5) which carries the deletion of F_0-F_1 ATPase. Then the three subunit proteins were overexpressed and co-purified as a complex ($MalFGK_2$) by affinity chromatography using a 6×histidine tag attached to the C-terminus of MalK as described previously (*6*). The modification of the protocol is that the cell pellet resuspension buffer contains 20 mM Tris (pH 8.0), 5 mM $MgCl_2$, 10% glycerol, and 0.4% n-Dodecyl-β-D-Maltopyranoside (DDM, Anatrace). Extracted $MalFGK_2$ was purified on cobalt Talon resin (Clontech) in buffer containing 20 mM Tris (pH 8.0), 100 mM NaCl, and 0.015% DDM. The eluted fractions were dialyzed overnight at 4℃ to remove imidazole and then followed by size-exclusion chromatography (Superdex 200, GE Healthcare). Proteins were concentrated with a Millipore filter with 100 kDa cut-off and stored in -80℃ until ready for use.

2.3.2 Expression, Purification and Spin Labeling of MBP

Wild-type or mutant MBP was cloned into pMCSG7 LIC vector, which encodes a 10xHis tag at the N-terminus of the protein, and then expressed in the *E. coli* strain BL21(DE3) Star. Cells were grown in Luria-Bertani medium at 37℃ to the midexponential phase and then the overexpression of MBP was induced by isopropyl-d-thiogalactoside at 22℃ for 20 hours. MBP was purified by cobalt-affinity chromatography in buffer containing 20 mM Tris-HCl pH 8.0 and 150 mM NaCl (2mM DTT was added for the cysteine mutants of MBP) and gel filtration (Superdex 75, GE

Healthcare) chromatography in buffer containing 10 mM Tris-HCl pH 8.0, 200 mM NaCl. To spin label the cysteine mutants of MBP (residue 41 and 271), 1 mL of a 200 μM solution of purified MBP was pretreated with 200 μM DTT to break any non-physiological MBP dimers formed due to the oxidizing environment of the cobalt affinity resin, then incubated with 2 mM MTSL and 500 μL nickel-Sepharose 6 Fast Flow resin (GE Healthcare) overnight with gentle shaking at 4 ℃. The resin was collected in a column, washed with a buffer containing 20 mM Tris-HCl at pH 8.0 with 100mM NaCl and 1mM EDTA to remove excess spin label.

2.3.3 Expression, Purification, and Removal of Histidine-tag of Membrane Scaffold Protein (MSP)

Expression and purification of a Membrane Scaffold Protein (MSP) for reconstituting nanodiscs with a diameter of 12.1 nm were performed as described before(*39*). In brief, the plasmid (pMSP1E3D1; Addgene) encoding for a polyhistidine-tagged MSP with TEV protease cleavage site at the N-terminus was transformed into *E. coli* strain BL21(DE3). 50ml of LB medium supplemented with 30 μg/mL kanamycin was used to grow cells. Till OD600 reached 0.6, the entire culture was transferred into a 500 mL TB medium (plus 30 μg/mL kanamycin) in a 2L flask. The culture was incubated at 37 °C, induced by 1mM IPTG isopropyl β-D-1-thiogalactopyranoside (IPTG) when the OD600 reached 2.5-3.0, and then centrifuged at 4,000 x g for 15 min at 4 ℃. The cell pellet was resuspended in 30 mL of 20 mM sodium phosphate buffer with pH of 7.4 containing 1 mM phenylmethylsulfonyl fluoride (PMSF, Sigma), 1% Triton X-100 (Sigma) and 30 mg/L DNAse I (Roche). Then cells were broken by passing the

resuspension through a high-pressure homogenizer (Emulsiflex-C5; Avestin) at 1500~2000 psi. Cell debris was removed by centrifugation at at 80,000 x g for 40 min at 4 ℃. The supernatant was mixed with pre-equilibrated Ni Sepharose 6 Fast Flow resin (GE Healthcare), for 1 hour with gentle rocking at 4 ℃. Then the mixture was loaded into a column, allowing the liquid to flow through, followed by 1) 10 column volume (CV) washes of Tris/HCl 40 mM pH 8, NaCl 0.3 M, Triton X-100 1%; 2) 5 CV washes of Tris/HCl 40 mM at pH 8, 0.3 M NaCl, 50 mM sodium cholate, 20 mM imidazole; and 3) 7 CV washes of 40 mM Tris/HCl at pH 8, 0.3 M NaCl, and 50 mM imidazole. MSP was eluted with 40 mM Tris-HCl at pH 8.0, 300 mM NaCl, and 400 mM imidazole. To store the uncut MSP, it was first dialyzed against 3.5 L of buffer A (20 mM Tris/HCl at pH 8 and 100 mM NaCl) at 4 ℃ and then frozen in -20 ℃. To cleave the N-terminus his-tag, before dialysis, MSP was incubated with TEV in the presence of 5 mM β-mercaptoethanol overnight and be passed through cobalt-affinity column to remove TEV protease and uncleaved MSP.

2.4 Reconstitution of $MalFGK_2$ in Nanodiscs

Nanodiscs represent a more native environment than liposomes, detergent micelles or bicelles and allow the study of purified membrane proteins with many techniques including size-exclusion chromatography, electron paramagnetic resonance, and analytical ultracentrifucation. Nanodiscs are soluble disk-shaped membrane patches. They contain a phospholipid bilayer encircled by a membrane scaffold protein. The $MalFGK_2$ was shown to recover its MBP-dependent ATP hydrolysis with little to no basal activity in both bicelles and nanodiscs (*39*). While both membrane mimics

represent alternative reconstitution systems for $MalFGK_2$, reconstitution in nanodiscs is more convenient than in bicelles and it is suitable for studying the transporter using size exclusion chromatography and electron paramagnetic resonance spectroscopy.

The nanodiscs were prepared using a certain ratio of soybean phospholipids: MSP: maltose transporter specified in corresponding sections. Cholate was added to solobilize the lipids. The final concentration of cholate was 25 mM, which is well above its critical micelle concentrations. The solubilized lipids, DDM-stabilized $MalFGK_2$ and purified MSP were mixed in a final volume of 250 μL in a microcentrifuge tube. The final concentrations of the maltose transporter and glycerol were 6 ~15 μM and < 3%, respectively. The assembly mixture was allowed to equilibrate for 1 hour at room temperature with gentle rocking. Then pre-washed biobeads SM-2 (BioRad) were dehydrated by vacuuming and were incubated with the mixture for 3 hours at room temperature with gentle rocking to trigger self-assembly of the nanodiscs by detergent removal. Then the bottom of the microcentrifuge tube was pierced. With a new microcentrifuge tube collecting the eluate, the microcentrifuge tube containing the mixture was spun at 1,000 ×g to separate the nanodiscs from the biobeads. Finally, the sample was spun at 10,000 ×g to remove any precipitates.

2.5 Size Exclusion Chromotography

The procedures of size-exclusion chromatography conducted in section 4.4 are described in (*33*). Samples (10 μL) in Buffer A were passed through a pre-equilibriated Superdex 200 5/150 size exclusion column (GE Healthcare) at room temperature at a flow rate of 0.1 mL/min using an AKTA purifier chromatography system. The void

volume was at 1.0 mL. The protein standards (Biorad) were (kDa): 670, 158, 44 and 17, which gave the following retention volumes (mL): 1.12, 1.56, 1.89 and 2.18, respectively.

The procedures conducted in other sections are described as the following. $MalFGK_2$ in buffer containing 20 mM Tris (pH 8.0), 100 mM NaCl, and 0.015% DDM.were passed through a Superdex 200 10/60 size-exclusion column and MBP in 20mM Tris-HCl 150mM NaCl buffer (pH 8) were injected into the Superdex 75 10/60 (for MBP) size-exclusion column (GE Healthcare). The column runs at 4 ℃ at a flow rate of 1 mL/min using an AKTA purifier chromatography system.

2.6 ATPase Activity Assay

A coupled ATP-regeneration system was used to measure the ATPase of the maltose transporter complex as described in (*3*). Briefly, besides the maltose transporter, the ATPase activity assay solution consists of 50 mM Hepes/KOH at pH 8.0, 10mM MgCl2, 4 mM phosphoenol pyruvate, 60 μg/ml pyruvate kinase, 32 μg/mL lactate dehydrogenase, 0.3 mM NADH and 1.5 mM ATP, in presence or absence of 150 μM maltose or MBP. The concentration of MBP will be specified in the later sections. Typically, 1 μg maltose transporter in nanodiscs assembly was added to a final volume of 70 μL for the assay. The amount of $MalF(\Delta P2)GK_2$ mutant used in the assay is 10 μg. A 5-min preincubation of the sample with ATPase activity assay reagents at room temperature was employed prior to the addition of ATP. The ATPase activity was measured at room temperature. Activity was reported as μmol of ATP hydrolyzed/min/mg of maltose transporter added to the reconstitution mixture for the nanodiscs.

2.7 Electron Paramagnetic Resonance (EPR)

X-band continuous wave (CW) EPR spectroscopy was carried out on a Bruker EMX-plus fitted with an ER4119HS cavity using WinEPR v4.40 as the computer interface. Sample volume was 30µl. The spectra were recorded at room temperature using 10 mW microwave power and 100 kHz modulation amplitude over 1.0 Gauss (G). Nine times over a 100 G scan width will be used. The spectra will be normalized to the same number of spins, calculated using Bruker WinEPR Processing, as the normalized double integral of the signal.

2.8 Analytical Ultracentrifugation (AUC)

The sedimentation coefficient, *s*, is described by the Svedberg equation:

$$s = \frac{v}{w_2 r} = \frac{M(1-\bar{v})}{Nf}$$

Where *v* is the velocity of the molecule, $\omega_2 r$ is the strength of the centrifugal field, *M* is the molecular mass, *f* is the frictional coefficient (which is directly related to macromolecular shape and size), ρ is the density of the solvent, *N* is Avogadro's number, and $\bar{v}$ is the partial specific volume of the solute.

In a high-speed sedimentation velocity experiment, the solute moves away from the air-solvent interface (i.e. the meniscus) to the bottom of the cell and forms a solute concentration gradient, named the boundary. The boundary sediments and diffuses with time and displays "boundary spreading" over the course of the experiment. The combination of the sedimentation and diffusion in the ultracentrifuge cell is described in terms of the flow, *J* (*40*):

$$J=sw_2rc-D(\partial c/\partial r)$$

where D is the diffusion coefficient, c is the solute concentration, and $\partial c/\partial r$ is the solute concentration gradient. In theory, the sedimentation velocity experiments can determine s and D (which is proportional to f). In the proposed research, M and D of the molecules are known. Considering two proteins with similar shape and size, the greater the molecular mass is, the bigger the sedimentation coefficient will be. In addition, concentration is positively correlated with UV280 which is detected during spinning. Given the relation of UV280 absorption versus s, we can quantify the amount of the nanodiscs of $MalFGK_2$ bound and unbound with MBP and finally plot the binding curve to obtain the dissociation constant.

2.9 Intrinsic Fluorescence Binding Assay

The binding assay is done in a fluorometer excited at 280nm, emitting at 344nm (*41*). The volume of the cuvette is 3mL. It is assumed that both gal-glu4 and MBP have 1:1 binding to MBP. The data are fitted with the equation (*42*):

$$f = [L]_{free} / (Kd + [L]_{free})$$

where *f* is the binding fraction,. *L* is the ligand and *Kd* is the dissociation constant.

CHAPTER 3. INITIAL INTERACTION BETWEEN MBP AND MALFG

3.1 Introduction

Usually, ABC transporters share a feature of substrate-bound binding protein (importers) or substrate (exporters) stimulation of the transporter ATPase activity, thus avoiding futile cycles of ATP hydrolysis and optimizing substrate transport efficiency. As an extensively-studied example, maltose transporter can be stimulated by maltose-bound MBP up to several-thousand fold. However, like other ABC transporters, the mechanism by which MBP stimulates the maltose transport is unclear.

MBP consists of two lobes, a C-lobe that contacts MalF and an N-lobe that binds MalG and the MalF-P2 loop (Figure 3.1). Previous EPR studies on C-lobe MBP in our lab (*33, 43*) have shown spectral broadening by EPR when maltose was added into the $MalFGK_2$ nanodiscs and spin-labeled MBP 41C/211C sample, indicating that maltose triggers MBP closure. However, how MBP first interacts with the transporter and why MBP stimulates ATP hydrolysis better with maltose than without remains unclear. Our hypothesis is that maltose enhances the interaction between MBP and maltose transporter. To test, the three interface regions between MBP and MalFG will be investigated by conducting EPR experiments with single spin label on MBP mutants.

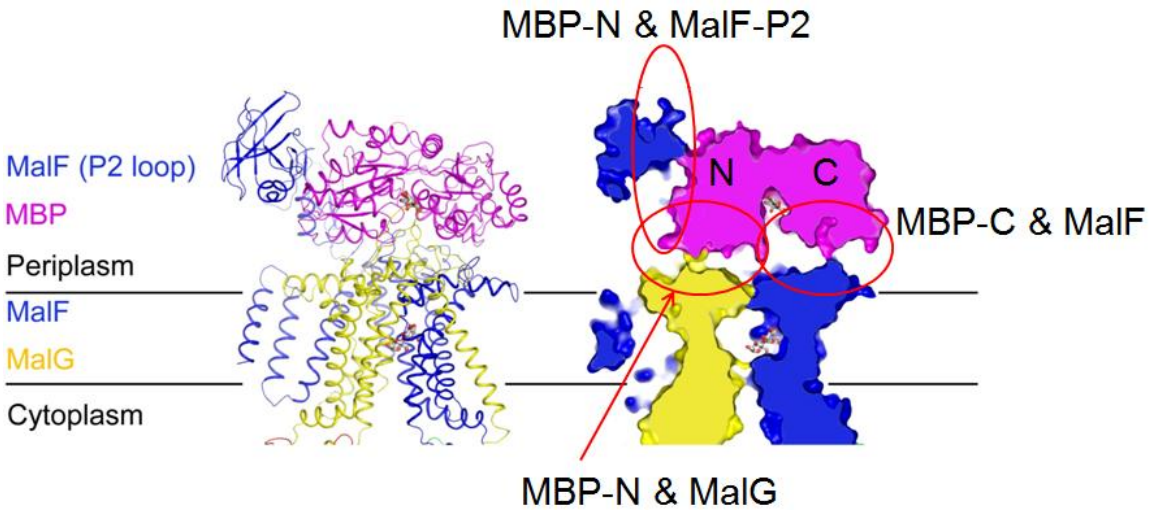

Figure 3.1 Three regions of interface between MBP and MalFG. A ribbon diagram (left) and a slab view (right) of the interacting regions between MBP (magenta) and MalF (blue) as well as between MBP and MalG (yellow) in the crystal structure (PBD ID: 3PV0). The interfaces are highlighted in red circles.

3.2 Initial interaction between MBP N-lobe and MalF-P2

To test the interaction between MBP N-lobe and MalF-P2 throughout the catalytic cycle, a cysteine mutant of MBP (MBP E274C) at the interface of P2 and MBP N-lobe was prepared for the EPR experiment. The MBP E274C mutant exhibited an *in vivo* transport positive phenotype on MacConkey agar with 1% maltose, suggesting that this mutant is able to uptake maltose. Spin-labeled MBP E274C was concentrated to 60 μM and stepped through the maltose transport cycle by successively adding 120 μM $MalFGK_2$ and the ligands as reported before (*43*). Ficoll alone was added to MBP mutants to simulate a decrease in the rate of tumbling that MBP would experience following interaction with the transporter (*44*).

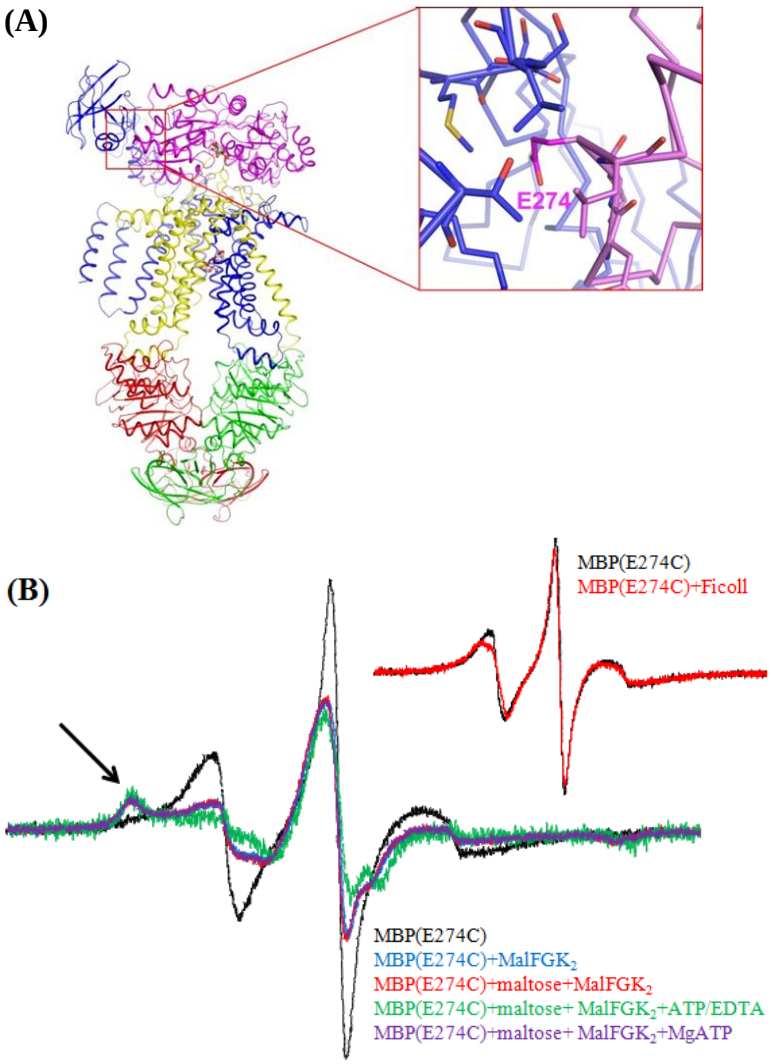

Figure 3.2 Interaction of MTSL-modified MBP E274C with $MalFGK_2$. (A) Location of MBP E274 in the maltose transporter (PBD ID: 3PV0). Colour codes: magenta, MBP; yellow, MalF; cyan, MalG; red and green, MalK dimer. MBP E274 is shown in an enlarged view in darker magenta. (B) The interaction with $MalFGK_2$ and the effect of maltose ligands. The small picture on the right shows the effect of Ficoll. MBP E274C was present at 50 μM and $MalFGK_2$ was stabilized in nanodiscs at 100 μM. The buffer contains no NaCl. EPR spectra are 100G wide. They are color coded according to the ligands, overlaid and normalized to the same number of spins.

The spectrum of MBP E274C and FicoII is very similar to that of MBP274C alone (Fig 1B), which indicated that the additional shoulder in the spectrum of MBP274C and

$MalFGK_2$ stabilized in nanodiscs results from the binding of MBP to $MalFGK_2$ instead of a change in the rate of molecular tumbling. Subtraction of the unbound MBP from the composite spectrum allowed us to estimate that 72% of MBP was bound to the transporter. There was little difference in the height of the immobile shoulder (see arrow) throughout the catalytic cycle by adding ligands, which suggests that there was little difference in the fraction of MBP bound with the transporter throughout the catalytic cycle. No change in the immobility was detected from the spectra upon the addition of maltose. This implies that maltose does not change the binding or conformation at the interface of P2 and MBP N-lobe. In addition, a slight increase in the immobility shoulder was observed upon the addition of ATP and EDTA, suggesting a more stable binding of P2 and MBP at the ATP-bound transition state (*6*). Addition of Mg^{2+} ion and ATP promoted ATP hydrolysis by $MalFGK_2$, followed by a return of the MBP E274C spectrum to overlap with that of maltose-bound MBP and MalFGK2 alone.

3.3 Initial interaction between MBP N-lobe and MalG

To investigate the initial interaction between MBP N-lobe and MalG, site 41 of MBP was mutated into cysteine and labeled for EPR. The MacConkey assay showed that the MBP D41C mutant supports maltose transport in the presence of the maltose transporter. Then the spin-labeled MBP D41C was concentrated to 60 μM for EPR experiments with $MalFGK_2$ in detergent and reconstituted in nanodiscs and the results were consistent.

The increase of viscosity by FicoII in the sample of MBP 41C and maltose did not cause any change in the shoulder of the spectrum (Figure 3.2B). This implies that any

change in the spectrum shoulder is caused by the more immobile environment of the backbone near the spin label site.

Upon the addition of $MalFGK_2$, the shoulder in the spectrum of MBP41C + maltose increased. When the spectrum of the MBP D41C mutant with maltose and $MalFGK_2$ was compared with the spectrum of the MBP D41C mutant with maltose alone (Figure 3.2B), it was clear that addition of $MalFGK_2$ resulted in a two-component spectrum. The more mobile component appeared to correspond to the unbound MBP, whereas the less mobile component (indicated with an arrow) corresponded to MBP bound to $MalFGK_2$ at the interface of MalG and MBP. It was estimated that 89% of the MBP was bound to MalG based on the subtraction of the unbound MBP from the composite spectrum. Addition of Vanadate Mg-ATP to mimic the transition state causes the percent bound MBP to increase to about 96% (*6*). The EPR spectra of MBP D41C and $MalFGK_2$ in nanodiscs in the presence or absence of maltose were compared (Figure 3.2C). A decrease in the mobility was observed upon the addition of maltose, indicating that substrate binding of MBP promotes the docking of MBP N-lobe onto MalG.

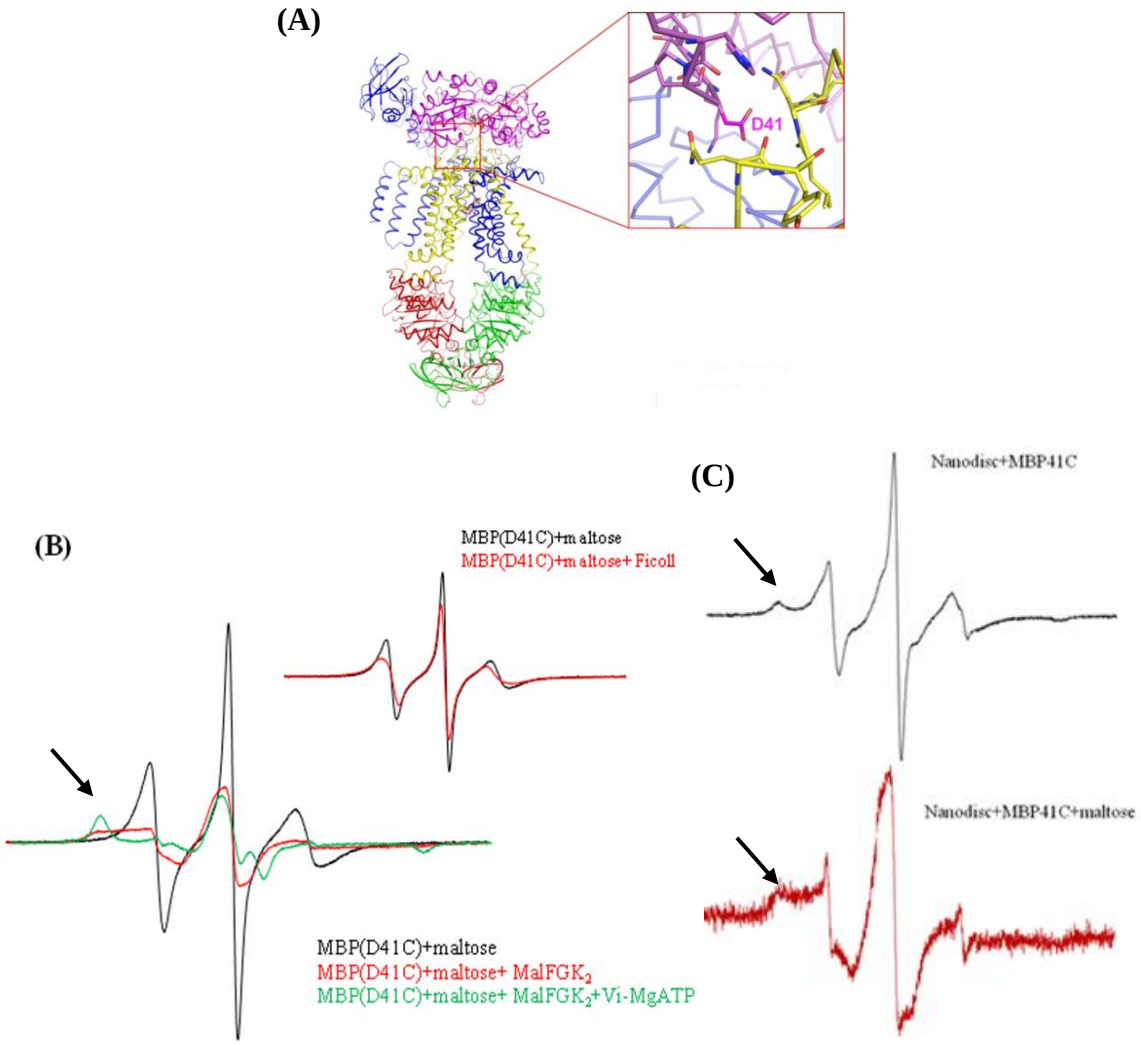

Figure 3.3 Interaction of MTSL-modified MBP D41C with $MalFGK_2$. (A) Location of MBP D41 in the maltose transporter (PBD ID: 3PV0). Colour codes: magenta, MBP; yellow, MalF; cyan, MalG; red and green, MalK dimer. MBP D41 is shown in an enlarged view in darker magenta. (B) The interaction of MBP41C with $MalFGK_2$ and the effect of maltose ligands. The small picture on the right shows the effect of Ficoll. MBP E41C was present at 50 μM and 100 μM $MalFGK_2$ was stabilized in 0.01% DDM. (C) The effect of maltose on 50 μM MBP41C and 100 μM $MalFGK_2$ stabilized in nanodiscs. The buffer in (B) and (C) contains no NaCl. EPR spectra are 100G wide and are overlaid with colors that are coded according to the ligands added. EPR spectra in (B) are normalized to the same number of spins while spectra in (C) are normalized to the maximum amplitude.

In agreement with literature, the signal of the immobile component increased upon the addition of the transporter to MBP D41C (Figure 3.2B), indicating that MBP

docks onto the transporter and changed the mobility at site 41 (*43*). However, the percent of MBP bound in Figure 3.2B is higher than that reported in the literature (about 89% versus 60%). A viable explanation for this discrepancy is the different concentrations of MBP and the transporter used.

In contrast to the decrease in mobility upon addition of maltose in Figure 3.2C, previous literature showed that no significant change in the mobility at position 41 upon the addition of maltose to MBP41C and $MalFGK_2$ (*43*). The possible explanation is that NaCl concentration is different. The buffer in this study contained no NaCl whereas the buffer in previous studies contained 150mM NaCl. The higher concentration of NaCl likely weakened the electrostatic interaction between MBP and the transporter to such an an extent that the interaction signal was not detected.

3.4 Initial interaction between MBP C-lobe and MalF

In the previous two sections, initial interaction between two regions of MBP N-lobe and MalFG were reported. This section reports on the interaction between MBP C-lobe and MalF. The EPR experiments on MBP C-lobe was majorly performed by Dr. Frances J.D. Alvarez (*45*). I helped her do some of the experiments.

The spectra of MBP 345C changed similarly slightly upon the addition of transporter as upon the addition of 20% Ficoll. In addition, no obvious difference was observed upon the addition of maltose. These suggested that the majority of MBP C-lobe does not dock onto the maltose transporter without nucleotide. Different from our EPR results, the C-lobe of MBP in the pre-translocation structure crystallized is on the maltose transporter.

A rational explanation for this difference is that MBP is in equilibrium between association and dissociation with the maltose transporter and crystal structure can only represent the one conformation that favors crystal packing. In contrast, EPR is able to represent real equilibrium in its natural environment. These can be supported by the fact that the pre-translocation complex cannot be co-purified by gel purification, probably because of weak binding between MBP and the maltose transporter in the presence of maltose alone. This suggests that the pre-translocation crystal structure is not the most stable conformation in solution.

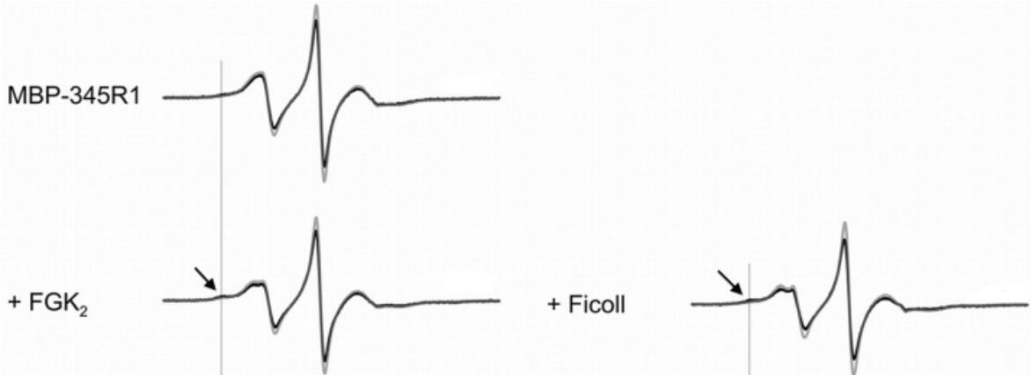

Figure 3.4 Interaction of MTSL-modified MBP 345C with $MalFGK_2$. Left, the interaction of MBP 345C with $MalFGK_2$. Right, the effect of Ficoll on the ERP spectra of MBP 345C. The EPR spectra are 100G wide and are overlaid. EPR spectra in are normalized to the same number of spins. MBP was present at 60 μM and MalFGK2 at 120 μM. Ligands were added at the concentrations specified in chapter 2. All experiments with MalFGK2 present were performed in detergent (DDM) solution. The spectra recorded without (black) or with (grey) maltose are overlaid.

3.5 Discussion

Previous studies reported the importance of periplasmic regions in MBP-stimulated maltose transport by showing that three mutations on these loops partially restore transport of a maltose-negative mutant (MalK Q140K) that was impaired in MBP-stimulated ATPase activity (*28*). Among these periplasmic loops, P2 is unique to Enterobacteriaceae maltose transporter (*46*). In agreement with previous NMR and

crosslinking studies (*24, 47*), we found that P2 is in close contact with MBP N-lobe throughout the catalytic cycle (Figure 3.1B), suggesting P2 is important in recruiting of MBP.

Maltose induces a more immobile interaction between MalG and MBP at site 41(Figure 3.2C). P3, a loop of MalG, is one periplasmic loop at the interface of MBP N-lobe and MalG, which was demonstrated to be important in substrate translocation from MBP to MalFG by "scooping" maltose out of the MBP maltose binding site and blocking the rebinding of maltose to MBP (*48*). The increase of immobility at the interface of P3 and MBP might result from a conformational change of P3 upon the addition of maltose and thus we suspect that MalG-P3 might be sensitive to substrate binding. In addition, in agreement with the vanadate trapping studies (*26*), the increase in immobility at both site 274 and 41 suggests a more stable binding of MBP and $MalFGK_2$ at transition state (Figure 3.1B and Figure 3.2B).

In summary, three regions of MBP were spin-labeled and the spin label mobility was studied. MBP N-lobe interacts with MalF-P2 throughout the transport cycle; mobility decreases upon the addition of maltose at the spin label site of 41 suggesting stronger interaction between MBP N-lobe and MalG; mobility did not change significantly at the spin label site 345 indicating no significant change in interaction between MBP C-lobe and MalF. These suggest that maltose enhances initial interaction between MBP and the transporter by promoting N-lobe interaction, which explains why maltose-bound MBP stimulates transporter more efficiently than maltose-free MBP. Although P2 maintains a close contact with MBP N-lobe throughout the catalytic cycle, the exact role of P2 is unclear. In the next chapter, we investigated the functional effect of P2 truncation.

CHAPTER 4. FUNCTIONAL STUDY OF MALF-P2

4.1 Introduction

In literature, it was reported that isolated P2 can fold independently of the transporter complex and the P2-MBP dissociation constant determined by isothermal titration calorimetry experiments is on the order of 10-20 μM, similarly in the presence or absence of maltose (*47*). Since the binding affinity of the intact maltose transporter is also in the micromolar range, the authors proposed that P2 is sufficient to bind MBP (*47*). Recently, further investigation was reported on the effect of isolated P2 on MBP (*49*). A third conformation is adopted by the maltose-bound MBP in the presence of P2 that is distinct from the closed maltose-bound MBP and open maltose-free MBP (*49*). Increased solvation rates for residues in the substrate-binding pocket were observed upon the addition of P2 by solvent-PRE measurements, further indicating a change in the solvent accessibility of the maltose-binding cleft in the presence of P2 (*49*). These data indicate that a possible third conformation of MBP induced by P2 could be a semi-open conformation which might play an important role in the activation of substrate transport by stabilizing the complex during the catalytic cycle. However, due to the lack of other contact interfaces between MBP and MalFG, the interaction between the isolated P2 and MBP may not work the same way as when it is part of the intact maltose transporter. Besides, the periplasmic loops among other bacterial maltose ABC transporters are much

shorter and are missing in homologous systems from Gram positive bacteria and archaea, where MBP is tethered to the membrane. Therefore, it is likely that P2 in the actual complex of maltose transporter in *E. coli* may function differently from the study of isolated P2. The EPR studies in Chapter 3 have demonstrated that P2 is important in recruiting MBP and MBP movement. To test whether P2 has additional important functions, a truncation that replaces P2 with a short GSGSG linker was constructed in both the wild-type maltose transporter and one BPI maltose transporter to carry out *in vivo* and *in vitro* assays. The linker is for the purpose of maintaining the natural structure of the maltose transporter after deleting P2 by linking the two segments of MalF.

4.2 Effect of P2 truncation on Maltose *Transport In Vivo*

Maltose transport of the P2-deleted maltose transporter mutant MalF(ΔP2)GK_2 (section 2.1) was tested by *in vivo* MacConkey assay. We showed that the mutant exhibits an *in vivo* transport negative phenotype on maltose MacConkey agar (Table 4.1). This indicated that deletion of P2 prevents maltose transport in *E. coli*. This agrees with previous report on the maltose uptake deficient phenotype of four MalF-P2 mutants (*46*), which indicated that P2 is necessary for maltose transport conducted by the *E. coli* maltose transporter system. According to the literature, the binding affinity between the isolated MalF-P2 and MBP (about 10-20 μM) is similar to the Km of the MBP-stimulated ATPase of the wild-type maltose transporter, $MalFGK_2$ (*27, 47*). The significance of P2 in recruiting MBP is also supported by the EPR results of MBP E274C (Chapter 3). Thus a rational explanation for the dysfunction of MalF(ΔP2)GK_2 is that the binding affinity drops too low for MalF(ΔP2)GK_2 to bind MBP. The following sections describe how MalF(ΔP2)GK_2 was purified and characterized *in vitro*, and then tested whether the

substrate-stimulated ATPase can be compensated by increasing MBP concentration to 1mM。

Table 4.1 Characterization of *E. coli* maltose transporter mutants.

Strain AD126 with Complex Variant	**MacConkey Colony Color***
MalF(ΔP2)GK_2+MBP	White
MalF(ΔP2)GK_2, no MBP	White
MalFGK_2 (wild type)+MBP	Red
MalFGK_2 (wild type), no MBP	White
MalF500GK2, no MBP	Red
MalF500 (ΔP2) GK2, no MBP	Red

*Maltose-fermenting *E. coli* appears as red colonies on a MacConkey Agar with 1% maltose, indicating a successful maltose transport into the cell. The observation was made after 14-hour incubation at 37℃. The color of the colonies of each sample is uniformly red or white. Observation after 12-hour incubation of MalF500 (ΔP2) GK2, no MBP shows smaller red in the middle of the colony with white edges, indicating a slower maltose metabolic rate.

It is known that binding-protein independent (BPI) proteins are able to couple substrate transport and ATP hydrolysis in the absence of the periplasmic substrate binding protein. To verify whether deletion of P2 disrupts the catalytic cycle, a binding protein independent (BPI) mutant was introduced to the P2 truncation mutant of the maltose transporter and the name of this mutant is F500ΔP2GK2. Briefly, the mutations in MalF or MalG permits binding protein independent transport of maltose (*31*). Recall

that BPI can transport maltose without MBP. A rational explanation of this is that the majority of BPI rests in a high energy intermediate conformation.

BPI is expected to maintain maltose transport function even in the absence of P2. F500 contains two site-mutations (G338R and N505I). The gene of malF500 with the P2 deleted, denoted malF500 (ΔP2) was constructed by mutagenesis. In the absence of MBP, F500 (ΔP2) exhibited an *in vivo* Mal^+ phenotype on maltose MacConkey agar after 14-hour incubation (Table 1). This showed that the binding-protein independent mutant, F500 can transport maltose without P2. In addition, comparing column 2 and 3 in Table 4.2, it took longer for the F500 (ΔP2) colonies to completely turn red than the F500 colonies. This indicates that the maltose transport of F500 is possibly slowed down by the deletion of P2 with the assumption that the expression level of F500 and F500 (ΔP2) are comparable. This assumption is based on similar numbers of colonies grown on the medium under the same conditions.

(A) (B)

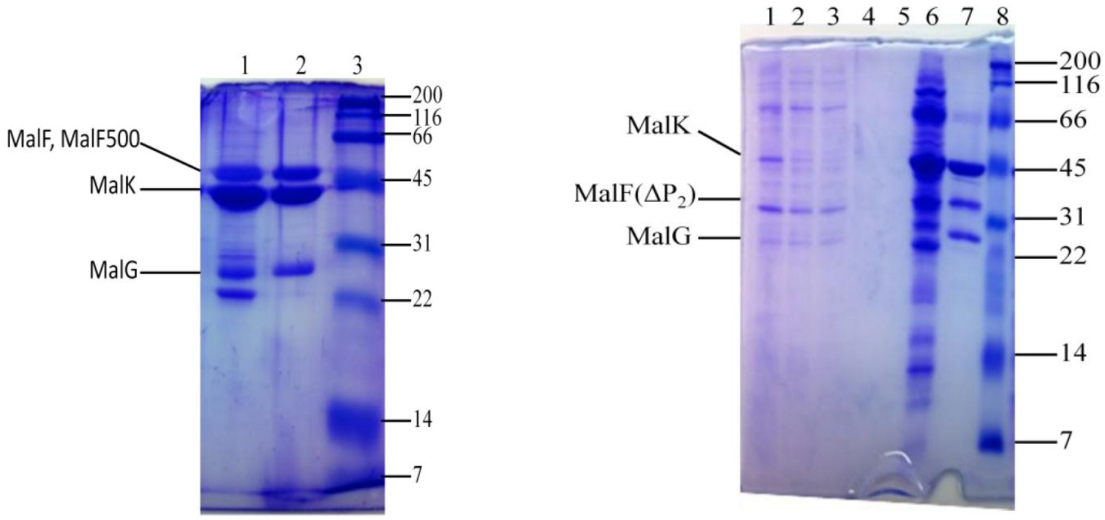

Figure 4.1 Maltose transporters visualized by 15% SDS-PAGE gels and Commassie staining. The (A) F500. Lane 1, F500. Lane 2, wild-type $MalFGK_2$. Lane 3, Molecular weight markers. (B) Fractions from steps of purification of F500 ΔP2 from the membrane. Lane 1, total membrane. Lane 2, Solubilized membrane. Lane 3, Cobalt unbound. Lane 4, 2 mM imidazole wash of cobalt resin. Lane 5, 5 mM imidazole wash of cobalt resin. Lane 6, 100 mM imidazole elution of cobalt resin. Lane 7, $MalF(\Delta P2)GK_2$. Lane 8, Molecular weight markers.

To further verify the role of P2 using the BPI mutant *in vitro*, different buffers were used to purify F500 and F500 ΔP2 GK2. F500 was successfully purified with the protocol described previously in section 2.2.1. However, the pure form of F500 ΔP2 GK2 could not be obtained (Figure 4.6). The band at the position of MalG is missing for the elution of F500(ΔP2) from cobalt resin, although there are bands at the right positions indicative of the presence of MalK and MalF500ΔP2. There are four possible reasons for a failure of membrane protein purification: (1) gene mutation due to some reasons like cell toxicity, (2) low expression level, (3) mislocation to the inclusion body, and (4) mis-folding or aggregation. The first possibility, unexpected gene mutation, can be ruled out since the gene sequences of malF500ΔP2 and malG were double checked after 24-hour

induction with 50 μM IPTG at 22℃. A more rational explanation is that either the expression level is too low or the mutant is misfolded.

4.3 Purification of MalF(ΔP2)GK_2

The protein purification protocol in Section 2.2 was modified to obtain stable and pure MalF(ΔP2)GK_2 mutant *in vitro*. High purity was achieved by using DDM in a buffer containing 50 mM Tris-HCl and 100 mM NaCl, at pH7. Purified MalF(ΔP2)GK_2 was first characterized on the 15% SDS-PAGE gel (Figure 4.1A). Three bands (lane 1) corresponding to three components of MalF(ΔP2)GK_2 were observed at the right position with a reference of the positions of the three bands of wild-type MalFGK_2 (lane 3). A sharp symmetrical profile of purified MalF(ΔP2)GK_2 in the size-exclusion chromatography analysis (Figure 4.1B) suggested that MalF(ΔP2)GK_2 is reconstituted as a complex and is well folded. To test whether the dysfunction of MalF(ΔP2)GK_2 is due to lack of interaction with MBP, MalF(ΔP2)GK_2 was stabilized in nanodiscs with optimized lipid:Membrane Scaffold Protein (MSP):MalFGK_2 ratio to mimic the membrane environment (section 4.4) and then ATP ase activity was measured with up to 1mM MBP (section 4.5).

(A)

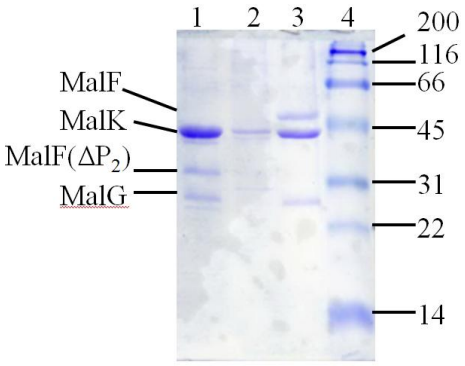

(B)

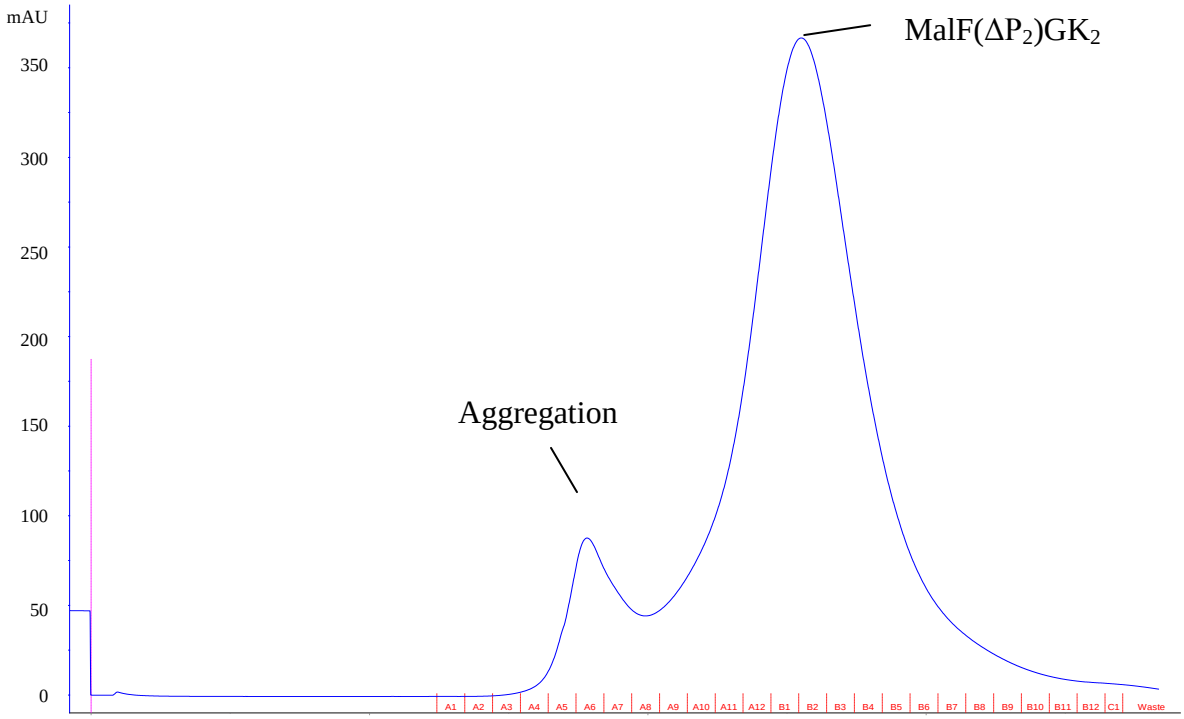

Figure 4.2 Purification of MalF(ΔP2)GK_2. (A) MalF(ΔP2)GK_2 visualized by 15% SDS-PAGE. Lane 1, MalF(ΔP2)GK_2. Lane 2, an example of an attempted purification of MalF(ΔP2)GK_2 under a different condition but showed only one band. Lane 3, MalFGK_2. Lane 4, Molecular weight markers. (B) The elution profile of the gel filtration column.

4.4 Functional Reconstitution of Nanodiscs

As outlined in Chapter 2, the nanodisc assembly mixture consists of the DDM-purified transporter, detergent solubilized soybean phospholipids and MSP. Previous literature indicated that one transporter per nanodiscs is better than two per nanodiscs because the former one displays higher ATPase activity, and that the MSP:$MalFGK_2$ ratio needs to be above 5:1 (w/w) to make the major fraction be one transporter per nanodiscs (*39*). To optimize the ATPase activity, the lipid:MSP:$MalFGK_2$ ratios were varied to reconstitute the nanodiscs assembly and then characterized with size-exclusion chromatography, analytical ultracentrifugation as well as ATPase activity assay.

Nanodiscs were prepared with 50:1 (w/w) lipid to MSP and with MSP to $MalFGK_2$ varying from 20:1 to 5:1 (w/w). The crude assembly was analyzed with size-exclusion chromatography (Figure 4.2 D-F). With reference to the elution volumes of standard proteins with known molecular weight described in section 2.5, the component that contains one transporter per nanodisc appears to be the major symmetric peak eluted around 1.4 mL in the size-exclusion chromatography profile (Figure 4.2). The shoulders between 1.0~1.1 mL and around 1.6 mL are larger-size aggregation and smaller-size impurities, respectively. At either 10:1 or 20:1, the aggregation is minimal. As the MSP:$MalFGK_2$ ratio increases, the smaller-size impurities increases. A rational interpretation was that as the ratio of MSP: $MalFGK_2$ increases, the amount of empty nanodiscs with only MSP and lipid increases. Following affinity purification (Figure 4.2 (A) - (C)) the peaks are more symmetric but the yields are much lower than the crude samples. In sum, 10:1 MSP to $MalFGK_2$ can minimize the number of aggregation and

empty nanodiscs. To maintain yield and save proteins, we prefer to use the crude assembly instead of purifying the nanodiscs with affinity chromatography.

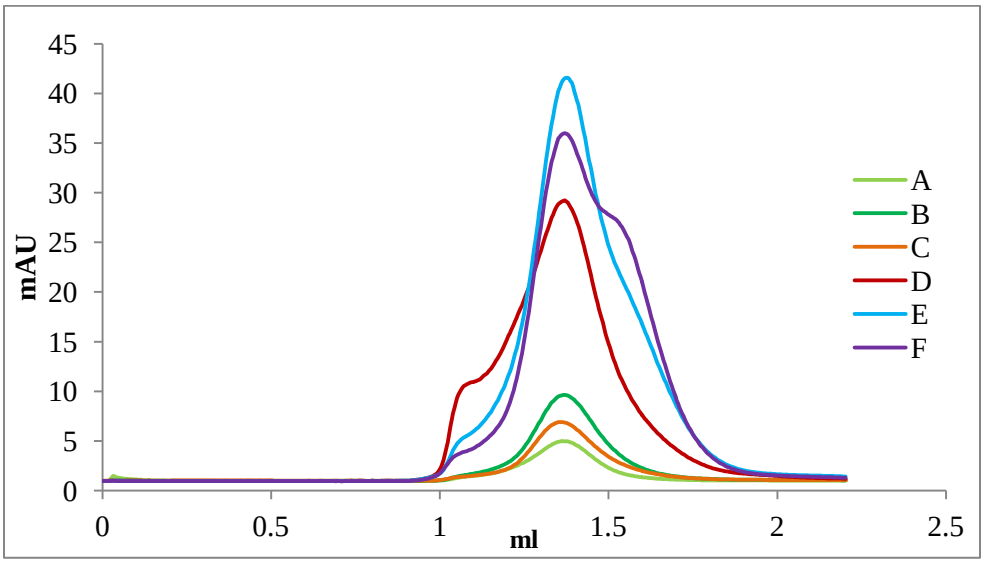

Figure 4.3 Nanodiscs size-exclusion profile with different MSP:MalFGK$_2$ ratios. (A) MSP:MalFGK$_2$=5, nanodiscs were purified with Ni affinity column; (B) MSP:MalFGK$_2$=10, nanodiscs were purified with Ni affinity column; (C) MSP:MalFGK$_2$=20, nanodiscs were purified with Ni affinity column; (D) MSP:MalFGK$_2$= 5, nanodiscs were the crude assembly that were not purified with Ni affinity column; (E) MSP:MalFGK2=10, nanodiscs were the crude assembly; (F) MSP:MalFGK$_2$= 20, nanodiscs were the crude assembly. MalFGK$_2$ concentration was approximately 6 μM. The lipid:MSP ratio was 50:1.

Previous literature showed that the ATPase activities of the nanodiscs varied less than 40% in the 50:1 to 120:1 (w/w) lipid:MSP range (*39*). In this study, a broader range of lipid:MSP ratio was investigated, from 500 to 5, corresponding to 2500 to 25 lipid:MalFGK$_2$. The functional reconstitution was evaluated by ATPase activity (Figure 4.3). Both the lipid:MalFGK$_2$ ratios of 250:1 and 500:1 showed high MBP-stimulated ATPase activity. Moreover, their low ATPase activity in the absence of maltose or MBP indicated that the complexes are well reconstituted.

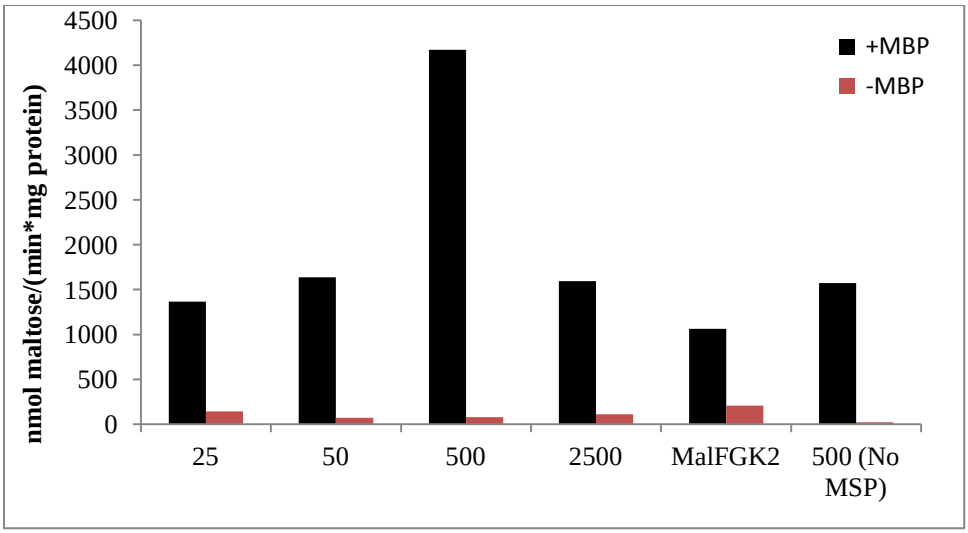

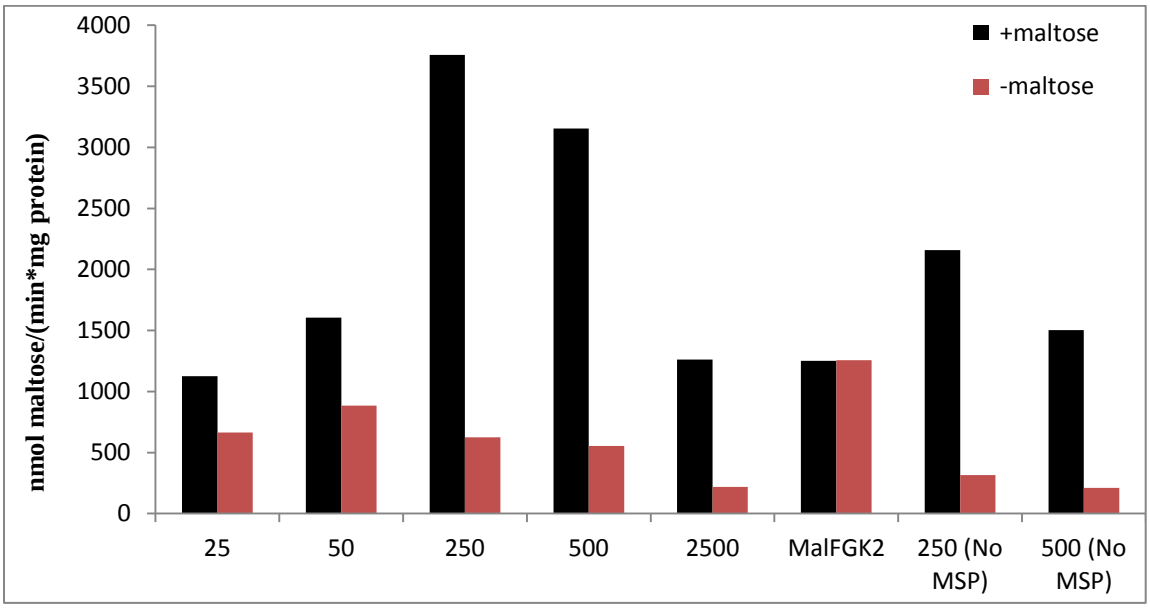

Figure 4.4 ATPase activity of nanodiscs with different lipid:$MalFGK_2$ ratios. Top, ATPase activity in the presence (black) or absence (red) of 5 μM MBP; bottom, ATPase activity in the presence (black) or absence (red) of 100 μM maltose. 6 μM $MalFGK_2$ were used in the assay. MSP: $MalFGK_2$ equaled to 5 for the samples in the presence of MSP. The number labeled at the bottom of each column indicates the ratio of lipid: $MalFGK_2$. The label "$MalFGK_2$" at the bottom of the columns means that $MalFGK_2$ was stabilized in 0.01% DDM without lipid or MSP.

To verify that the dominant component of the nanodiscs reconstituted are in the form of one transporter per two MSP, the major peak fraction of the nanodiscs in the size-exclusion chromatography profile was collected and concentrated to approximately 6 uM. The samples were analyzed by our collaborator Dr. Paul Lake with analytical ultracentrifugation. The ratio of lipid: $MalFGK_2$:MSP was fine-tuned according to the AUC profile of impurities and desired product intensity, among which the ratio of lipid:MSP:$MalFGK_2$ = 500:10:1 displayed the cleanest profile with two sharp major peaks (Figure 4.4). The two major peaks in the AUC profile corresponded to sedimentation coefficient 3.3 S and 9.4 S, respectively. The molecular weights of the two components are estimated to be 41 kDa and 204 kDa, respectively. Thus the left peak in Figure 4.4 represents MBP (43 kDa). The most likely interpretation of the right peak is the nanodiscs with one transporter (171 kDa) per two MSP (28 kDa). The molecular weight estimated from the sedimentration coefficient would be too small to represent two transporters per two MSP. No obvious higher order aggregates or smaller-size impurities were shown, indicating a successful optimization of the protocol to reconstitute one transporter with two MSP.

This section showed that lipid:MSP ratio falling in between 50-100:1 and MSP:maltose transporter ratio ranging from 5:1 to 10:1 are able to maximize the component of nanodiscs containing one transporter per two MSP and to maintain high level of MBP stimulated ATPase activity. Based on these results, lipid:MSP:maltose transporter = 100:5:1 was chosen to test whether increasing concentration of MBP up to 1mM.

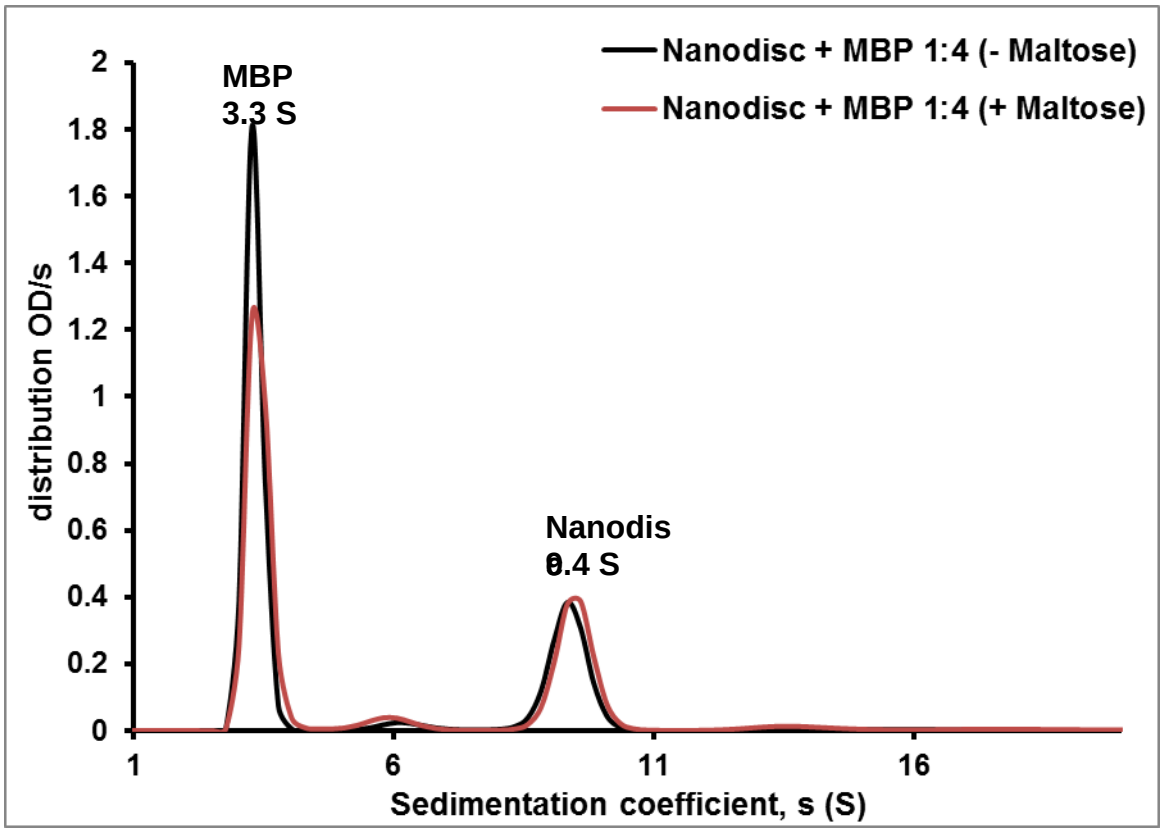

Figure 4.5 AUC profile of $MalFGK_2$ nanodiscs with and without maltose.

4.5 ATPase Activity of $MalF(\Delta P2)GK_2$ in Nanodiscs

From the previous two sections, the pure protein of $MalF(\Delta P2)GK_2$ was obtained *in vitro* and the functional nanodiscs reconstitution protocol with wild-type $MalFGK_2$ was optimized. The binding affinity of $MalF(\Delta P2)GK_2$ and MBP is too low to be measured directly. To verify that the dysfunction of the transporter by the truncation of P2 was due to the decrease of binding affinity with MBP, $MalF(\Delta P2)GK_2$ was reconstituted into nanodiscs and ATPase activity with a gradient of high concentrations of MBP was performed.

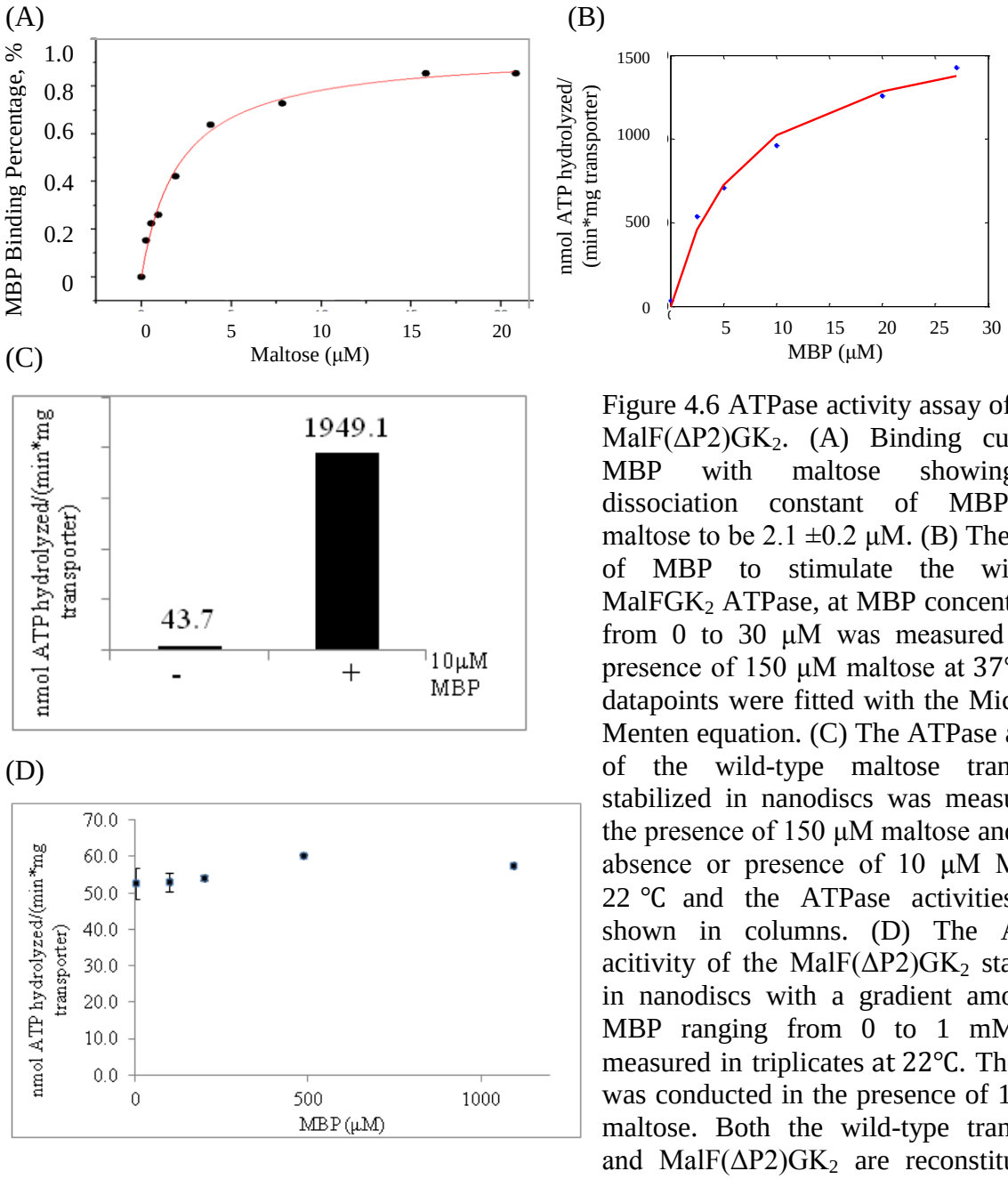

Figure 4.6 ATPase activity assay of MBP-MalF(ΔP2)GK_2. (A) Binding curve of MBP with maltose showing the dissociation constant of MBP with maltose to be 2.1 ±0.2 μM. (B) The ability of MBP to stimulate the wild-type $MalFGK_2$ ATPase, at MBP concentrations from 0 to 30 μM was measured in the presence of 150 μM maltose at 37℃. The datapoints were fitted with the Michaelis-Menten equation. (C) The ATPase activity of the wild-type maltose transporter stabilized in nanodiscs was measured in the presence of 150 μM maltose and in the absence or presence of 10 μM MBP at 22 ℃ and the ATPase activities were shown in columns. (D) The ATPase acitivity of the MalF(ΔP2)GK_2 stabilized in nanodiscs with a gradient amount of MBP ranging from 0 to 1 mM were measured in triplicates at 22℃. The assay was conducted in the presence of 150 μM maltose. Both the wild-type transporter and MalF(ΔP2)GK_2 are reconstituted in nanodiscs.

If recruiting MBP to the transporter is the sole role of P2, MBP-stimulation of ATPase should have displayed a Michaelis-Menten curve, the slope of which increased as the concentration MBP increased before saturation. The ATPase activity of MalF(ΔP2)GK_2 stabilized in nanodiscs with MBP ranging from 100 μM to 1 mM was measured in the presence of 150 μM maltose and 1.5 mM ATP at 22℃ (Figure 4.5D). The solubility of MBP in water is estimated to be about 5 mM. In addition, MBP increases the viscosity of the solution, thus making it hard to add high concentrations of MBP and mix the reagents in the solution. A MBP concentration of 1 mM is approximately the upper limit that can be used in the ATPase activity assay.

The ATPase activity of MalF(ΔP2)GK_2 in the presence of 1 mM MBP (57.7 nmol/mg/min) is less than 10% higher than that in the absence of MBP (52.7 nmol/mg/min) (Figure 4.5D). If this is explained by the fact that the Km for MalF(ΔP2)GK_2 is much higher than 1094 μM, the ATPase activity should still increase as the concentration of MBP increases from 0 to 1 mM, since the amount of MBP bound to the transporter increases as the amount of MBP increases before saturation. However, instead of a positive correlation between the ATPase activity and the concentration of MBP before saturation, the curve of the ATPase activity of MalF(ΔP2)GK_2 versus MBP concentration was flat. This indicated that the function of maltose transport is disabled by the deletion of P2. Regardless of no increase in the ATPase activity, MalF(ΔP2)GK_2 still displays an absolute value of 50 ~ 60 nmol/min/mg ATPase activity, suggesting that MalK dimer is still an active ATPase after truncation of P2.

As a control of MBP stimulation, the ability of MBP to stimulate the wild-type MalFGK_2 ATPase stabilized in the form of proteoliposome at MBP concentrations from

2.5 to 27 μM was measured in the presence of 150 μM maltose and 1.5 mM ATP at 37℃ (Figure 4.5B). The curve fits to the Michaelis-Menten equation which yielded Km value of approximately 7 uM, consistent with the reported Km value of about 15 uM (*27*). The nanodiscs reconstitution and the assay conditions were controlled by the wild-type maltose transporter nanodiscs. The ATPase activity of $MalFGK_2$ was 1949.1 nmol/mg/min in the presence of 10 μM MBP and 43.7 nmol/min/mg in the absence of MBP(Figure 4.5B), displaying a MBP-stimulation of about 45-fold, consistent with the literature (*27*). In addition, the background reading from MBP and the reagents for the ATPase activity assay was negligible.

To verify that the maltose concentration in the ATPase assay is abundant for MBP, the dissociation constant (K_d) of MBP with Maltose was determined by intrinsic fluorescence (Figure 4.5A) to be 2.11±0.22 μ M. This is consistent with the reported K_d (3 μ M) (*48, 50*). Thus, 150 μM maltose in the ATPase activity assay is abundant for MBP.

In summary, P2 loop deletion disrupted the MBP stimulation of ATPase activity of the maltose transporter complex, and it cannot be rescued by increasing maltose-MBP concentration up to 1mM.

4.6 Discussion

To test functions of P2, a mutant which has a replacement of P2 with a short GSGSG linker, $MalF(\Delta P2)GK_2$ was purified and characterized. Before testing ATPase activity assay with $MalF(\Delta P2)GK_2$ in nanodiscs, we optimized the functional reconstitution of the nanodiscs and physically characterized the components. Our result showed that

MSP:MalFGK$_2$ ratio should be 5:1 in order to minimize the amount of aggregation and empty nanodiscs in the crude nanodiscs. Lipid: MalFGK$_2$ should be 50~100:1 to maintain a high MBP-stimulated ATPase activity of MalFGK$_2$. The nanodiscs were demonstrated to contain one MalFGK$_2$ per two MSP by the sedimentation coefficient of the assembly.

In agreement with the ability of MalF(ΔP2)GK$_2$ to be co-crystalized with EIIA^{Glc}, our results suggest that the MalF(ΔP2)GK$_2$ is well-folded. However, the function of MalFGK$_2$ was disabled by the deletion of P2 (Table 4.1). Wild-type MalFGK$_2$ reaches the maximal ATPase activity with only 20-25 μM MBP. However, no MBP-stimulated ATPase activity of MalF(ΔP2)GK$_2$ was detected even in the presence of 1 mM MBP (Figure 4.5). This may due to the increase in Km to such an extent that 1 mM MBP cannot bind MalF(ΔP2)GK$_2$. Nevetheless, this study indicated that MalFGK$_2$ cannot interact with MBP in the absence of P2. And it suggested a possible role of the interaction between P2 and MBP in inducing or stabilizing a high-energy intermediate conformation of the maltose transporter between resting state and transition state. To further test which steps in maltose transport catalytic cycle the interaction of P2 and MBP are responsible for, we constructed a P2-deleted mutant on F500.

Binding-protein independent proteins, however, do not need MBP to transport maltose into the cell (section 1.5). A rational explanation for the independence of MBP for our study is that the resting state of BPI is distablized and that the majority of the BPI mutant rests in a high-energy intermediate that can easily proceed to the out-ward facing transition state conformation without the assistance of MBP (*19, 25, 36*), Based on this assumption, we hypothesized that F500 is able to transport maltose without P2, which was verified by the *in vivo* MacConkey assay (Table 4.2). Consistently, the crosslink data

from Dr. Shanshuang Chen revealed that the maltose transporter is able to function when it is crosslinked with MBP whereas lowering the local concentration of MBP by breaking the disulfide bond between MBP and the transporter with DTT reduced ATPase activity (*24*). Together with our finding that the MBP-P2 interaction is maintained throughout the catalytic cycle and that F500 can function after P2 truncation, it is likely that P2 is only involved in recruiting MBP.

Recent NMR studies have shown that the binding of P2 induces a semi-open state of MBP both in the presence and absence of maltose (*49*). Conflicting results are found in the pre-T state crystal structure in which MBP is not semi-open (*19*). This discrepancy may due to the lack of interactions between MBP and other extracytoplasmic loops of MalFG when using an isolated P2. Nevertheless, the possibility that MBP-P2 interaction contributes to the conformational change from the resting state to the transition state cannot be completely ruled out.

To conclude, chapter 4 mainly reported that P2 truncation in wild-type results in loss of function whereas P2 domain is not essential for BPI mutant F500. It is possible that MBP-P2 interaction is significant in the conformational change from resting state to a high-energy intermediate, although no communication between 1 mM MBP and MalK might due to too low binding affinity of MalF(ΔP2)GK_2 to bind with MBP.

The current maltose transport model was modified based on the results in the thesis (Figure 4.7). MalF-P2 maintains close contact with MBP N-lobe throughout the cycle. Upon the addition of maltose, interaction between MalG short loops and MBP N-lobe becomes much stronger while interaction between MalF short loops and MBP C-lobe remains very weak.

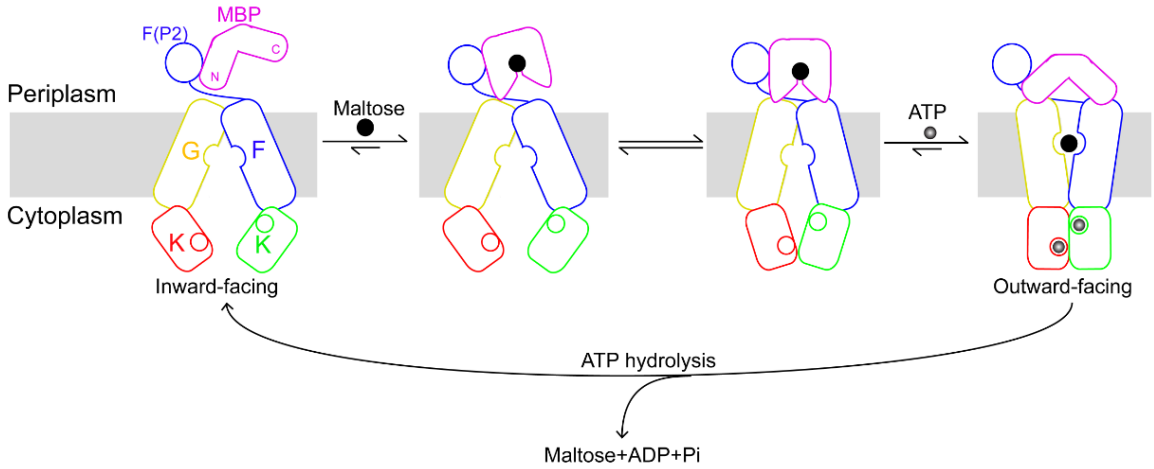

Figure 4.7 A Model of the *E.coli* maltose transporter catalytic cycle. The interaction between MBP and MalFG in the inward-facing conformation and in the intermediate conformations between inward-facing and outward-facing conformations are modified according to our results and the reported model (*19*). MBP N-lobe initially interacts with MalF-P2 even in the absence of maltose. Maltose triggers MBP closure and enhance the interaction between MBP N-lobe and MalG, while MBP C-lobe remains in equilibrium between associating and dissociating with MalF.

REFERENCES

REFERENCES

1. Lang, H., Jonson, G., Holmgren, J., and Palva, E. T. (1994) THE MALTOSE REGULON OF VIBRIO-CHOLERAE AFFECTS PRODUCTION AND SECRETION OF VIRULENCE FACTORS, *Infection and Immunity 62*, 4781-4788.
2. Shelburne, S. A., Davenport, M. T., Keith, D. B., and Musser, J. M. (2008) The role of complex carbohydrate catabolism in the pathogenesis of invasive streptococci, *Trends Microbiol. 16*, 318-325.
3. Orelle, C., Ayvaz, T., Everly, R. M., Klug, C. S., and Davidson, A. L. (2008) Both maltose-binding protein and ATP are required for nucleotide-binding domain closure in the intact maltose ABC transporter, *Proc. Natl. Acad. Sci. U. S. A. 105*, 12837-12842.
4. Davidson, A. L., Dassa, E., Orelle, C., and Chen, J. (2008) Structure, function, and evolution of bacterial ATP-binding cassette systems, *Microbiol. Mol. Biol. Rev. 72*, 317-364.
5. Garmory, H. S., and Titball, R. W. (2004) ATP-binding cassette transporters are targets for the development of antibacterial vaccines and therapies, *Infection and Immunity 72*, 6757-6763.
6. Oldham, M. L., Khare, D., Quiocho, F. A., Davidson, A. L., and Chen, J. (2007) Crystal structure of a catalytic intermediate of the maltose transporter, *Nature 450*, 515-U517.
7. Davidson, A. L., and Nikaido, H. (1990) OVERPRODUCTION, SOLUBILIZATION, AND RECONSTITUTION OF THE MALTOSE TRANSPORT-SYSTEM FROM *ESCHERICHIA-COLI*, *J. Biol. Chem. 265*, 4254-4260.
8. Davidson, A. L., and Nikaido, H. (1991) PURIFICATION AND CHARACTERIZATION OF THE MEMBRANE-ASSOCIATED COMPONENTS OF THE MALTOSE TRANSPORT-SYSTEM FROM *ESCHERICHIA-COLI*, *J. Biol. Chem. 266*, 8946-8951.
9. Horlacher, R., Xavier, K. B., Santos, H., DiRuggiero, J., Kossmann, M., and Boos, W. (1998) Archaeal binding protein-dependent ABC transporter: Molecular and biochemical analysis of the trehalose/maltose transport system of the hyperthermophilic archaeon Thermococcus litoralis, *J. Bacteriol. 180*, 680-689.
10. Ehrmann, M., Ehrle, R., Hofmann, E., Boos, W., and Schlosser, A. (1998) The ABC maltose transporter, *Mol. Microbiol. 29*, 685-694.

11. Ehrmann, M., and Beckwith, J. (1991) PROPER INSERTION OF A COMPLEX MEMBRANE-PROTEIN IN THE ABSENCE OF ITS AMINO-TERMINAL EXPORT SIGNAL, *J. Biol. Chem. 266*, 16530-16533.
12. Hulsmann, A., Lurz, R., Scheffel, F., and Schneider, E. (2000) Maltose and maltodextrin transport in the thermoacidophilic gram-positive bacterium Alicyclobacillus acidocaldarius is mediated by a high-affinity transport system that includes a maltose binding protein tolerant to low pH, *J. Bacteriol. 182*, 6292-6301.
13. Chen, J., Lu, G., Lin, J., Davidson, A. L., and Quiocho, F. A. (2003) A tweezers-like motion of the ATP-binding cassette dimer in an ABC transport cycle, *Mol Cell 12*, 651-661.
14. Kennedy, K. A., and Traxler, B. (1999) MalK forms a dimer independent of its assembly into the MalFGK2 ATP-binding cassette transporter of *Escherichia coli*, *J Biol Chem 274*, 6259-6264.
15. Dean, D. A., Hor, L. I., Shuman, H. A., and Nikaido, H. (1992) INTERACTION BETWEEN MALTOSE-BINDING PROTEIN AND THE MEMBRANE-ASSOCIATED MALTOSE TRANSPORTER COMPLEX IN *ESCHERICHIA-COLI*, *Mol. Microbiol. 6*, 2033-2040.
16. Manson, M. D., Boos, W., Bassford, P. J., and Rasmussen, B. A. (1985) DEPENDENCE OF MALTOSE TRANSPORT AND CHEMOTAXIS ON THE AMOUNT OF MALTOSE-BINDING PROTEIN, *J. Biol. Chem. 260*, 9727-9733.
17. Hunke, S., Drose, S., and Schneider, E. (1995) VANADATE AND BAFILOMYCIN A(1) ARE POTENT INHIBITORS OF THE ATPASE ACTIVITY OF THE RECONSTITUTED BACTERIAL ATP-BINDING CASSETTE TRANSPORTER FOR MALTOSE (MALFGK(2)), *Biochemical and Biophysical Research Communications 216*, 589-594.
18. Sharma, S., and Davidson, A. L. (2000) Vanadate-induced trapping of nucleotides by purified maltose transport complex requires ATP hydrolysis, *J. Bacteriol. 182*, 6570-6576.
19. Oldham, M. L., and Chen, J. (2011) Crystal Structure of the Maltose Transporter in a Pretranslocation Intermediate State, *Science 332*, 1202-1205.
20. Chen, J., Oldham, M., Khare, D., and Davidson, A. L. (2009) ALTERNATING ACCESS IN THE MALTOSE ABC TRANSPORTER, *J. Physiol. Sci. 59*, 116-116.
21. Schmees, G., Stein, A., Hunke, S., Landmesser, H., and Schneider, E. (1999) Functional consequences of mutations in the conserved 'signature sequence' of the ATP-binding-cassette protein MalK, *Eur. J. Biochem. 266*, 420-430.
22. Orelle, C., Alvarez, F. J. D., Oldham, M. L., Orelle, A., Wiley, T. E., Chen, J., and Davidson, A. L. (2010) Dynamics of alpha-helical subdomain rotation in the intact maltose ATP-binding cassette transporter, *Proc. Natl. Acad. Sci. U. S. A. 107*, 20293-20298.
23. Covitz, K. M. Y., Panagiotidis, C. H., Hor, L. I., Reyes, M., Treptow, N. A., and Shuman, H. A. (1994) MUTATIONS THAT ALTER THE TRANSMEMBRANE SIGNALING PATHWAY IN AN ATP BINDING CASSETTE (ABC) TRANSPORTER, *Embo J. 13*, 1752-1759.

24. Chen, S. (2013). REGULATION MECHANISM AND SUBSTRATE SPECIFICITY OF THE *ESCHERICHIA COLI* MALTOSE TRANSPORTER (doctoral dissertation). Purdue University, West Lafayette, IN.
25. Shilton, B. H. (2008) The dynamics of the MBP-MalFGK(2) interaction: A prototype for binding protein dependent ABC-transporter systems, *Biochimica Et Biophysica Acta-Biomembranes 1778*, 1772-1780.
26. Chen, J., Sharma, S., Quiocho, F. A., and Davidson, A. L. (2001) Trapping the transition state of an ATP-binding cassette transporter: Evidence for a concerted mechanism of maltose transport, *Proc. Natl. Acad. Sci. U. S. A. 98*, 1525-1530.
27. Gould, A. D., Telmer, P. G., and Shilton, B. H. (2009) Stimulation of the Maltose Transporter ATPase by Unliganded Maltose Binding Protein, *Biochemistry 48*, 8051-8061.
28. Daus, M. L., Berendt, S., Wuttge, S., and Schneider, E. (2007) Maltose binding protein (MalE) interacts with periplasmic loops P2 and P1 respectively of the MalFG subunits of the maltose ATP binding cassette transporter (MalFGK(2)) from *Escherichia coli* Salmonella during the transport cycle, *Mol. Microbiol. 66*, 1107-1122.
29. Shuman, H. A. (1982) ACTIVE-TRANSPORT OF MALTOSE IN *ESCHERICHIA-COLI*-K12 - ROLE OF THE PERIPLASMIC MALTOSE-BINDING PROTEIN AND EVIDENCE FOR A SUBSTRATE RECOGNITION SITE IN THE CYTOPLASMIC MEMBRANE, *J. Biol. Chem. 257*, 5455-5461.
30. Treptow, N. A., and Shuman, H. A. (1985) GENETIC-EVIDENCE FOR SUBSTRATE AND PERIPLASMIC-BINDING-PROTEIN RECOGNITION BY THE MALF AND MALG PROTEINS, CYTOPLASMIC MEMBRANE-COMPONENTS OF THE *ESCHERICHIA-COLI* MALTOSE TRANSPORT-SYSTEM, *J. Bacteriol. 163*, 654-660.
31. Davidson, A. L., Laghaeian, S. S., and Mannering, D. E. (1996) The maltose transport system of *Escherichia coli* displays positive cooperativity in ATP hydrolysis, *J. Biol. Chem. 271*, 4858-4863.
32. Bajaj, R., Park, M. I., Paul, L. N., Klug, C. S., and Davidson, A. L. (2013) Structural Mechanism of Action of Binding Protein Independent Mutant MalG511 of *Escherichia Coli* Maltose Transporter, *Biophys. J. 104*, 111A-111A.
33. Alvarez, D. (2011). CONFORMATIONAL DYNAMICS OF THE MALTOSE TRANSPORTER IN *ESCHERICHIA COLI* (doctoral dissertation). Purdue University, West Lafayette, IN.
34. Dean, D. A., Hor, L. I., Shuman, H. A., and Nikaido, H. (1992) Interaction between maltose-binding protein and the membrane-associated maltose transporter complex in *Escherichia coli*, *Mol Microbiol 6*, 2033-2040.
35. Daus, M. L., Landmesser, H., Schlosser, A., Muller, P., Herrmann, A., and Schneider, E. (2006) ATP induces conformational changes of periplasmic loop regions of the maltose ATP-binding cassette transporter, *J. Biol. Chem. 281*, 3856-3865.
36. Mannering, D. E., Sharma, S., and Davidson, A. L. (2001) Demonstration of conformational changes associated with activation of the maltose transport complex, *J. Biol. Chem. 276*, 12362-12368.

37. Austermuhle, M. I., Hall, J. A., Klug, C. S., and Davidson, A. L. (2004) Maltose-binding protein is open in the catalytic transition state for ATP hydrolysis during maltose transport, *J Biol Chem 279*, 28243-28250.
38. Miller, J. H. (1972) *Experiments in molecular genetics*, 3rd, illustrated ed., Cold Spring Harbor Laboratory.
39. Alvarez, F. J. D., Orelle, C., and Davidson, A. L. (2010) Functional Reconstitution of an ABC Transporter in Nanodiscs for Use in Electron Paramagnetic Resonance Spectroscopy, *J. Am. Chem. Soc. 132*, 9513-9515.
40. Cole, J. L., and Hansen, J. C. (1999) Analytical ultracentrifugation as a contemporary biomolecular research tool, *Journal of biomolecular techniques : JBT 10*, 163-176.
41. Miller, D. M., Olson, J. S., Pflugrath, J. W., and Quiocho, F. A. (1983) RATES OF LIGAND-BINDING TO PERIPLASMIC PROTEINS INVOLVED IN BACTERIAL TRANSPORT AND CHEMOTAXIS, *J. Biol. Chem. 258*, 3665-3672.
42. Szmelcman, S., Schwartz, M., Silhavy, T. J., and Boos, W. (1976) MALTOSE TRANSPORT IN *ESCHERICHIA-COLI*-K12 - COMPARISON OF TRANSPORT KINETICS IN WILD-TYPE AND LAMBDA-RESISTANT MUTANTS WITH DISSOCIATION-CONSTANTS OF MALTOSE-BINDING PROTEIN AS MEASURED BY FLUORESCENCE QUENCHING, *Eur. J. Biochem. 65*, 13-19.
43. Austermuhle, M. I., Hall, J. A., Klug, C. S., and Davidson, A. L. (2004) Maltose-binding protein is open in the catalytic transition state for ATP hydrolysis during maltose transport, *J. Biol. Chem. 279*, 28243-28250.
44. Lopez, C. J., Fleissner, M. R., Guo, Z., Kusnetzow, A. K., and Hubbell, W. L. (2009) Osmolyte perturbation reveals conformational equilibria in spin-labeled proteins, *Protein Sci 18*, 1637-1652.
45. Alvarez, F. J. D., Orelle, C., Klug, C. S., and Davidson, A. L. (2011) Both Lobes of Maltose Binding Protein are Engaged in Stabilization of the Semi-Open State of the Malk Dimer in the Maltose ABC Transporter, *Biophys. J. 100*, 134-134.
46. Tapia, M. I., Mourez, M., Hofnung, M., and Dassa, E. (1999) Structure-function study of MalF protein by random mutagenesis, *J. Bacteriol. 181*, 2267-2272.
47. Jacso, T., Grote, M., Daus, M. L., Schmieder, P., Keller, S., Schneider, E., and Reif, B. (2009) Periplasmic Loop P2 of the MalF Subunit of the Maltose ATP Binding Cassette Transporter Is Sufficient To Bind the Maltose Binding Protein MalE, *Biochemistry 48*, 2216-2225.
48. Cui, J. M., Qasim, S., and Davidson, A. L. (2010) Uncoupling Substrate Transport from ATP Hydrolysis in the *Escherichia coli* Maltose Transporter, *J. Biol. Chem. 285*, 39986-39993.
49. Jacso, T., Schneider, E., Rupp, B., and Reif, B. (2012) Substrate Transport Activation Is Mediated through Second Periplasmic Loop of Transmembrane Protein MalF in Maltose Transport Complex of *Escherichia coli*, *J. Biol. Chem. 287*, 17040-17049.

50. Martineau, P., Szmelcman, S., Spurlino, J. C., Quiocho, F. A., and Hofnung, M. (1990) GENETIC APPROACH TO THE ROLE OF TRYPTOPHAN RESIDUES IN THE ACTIVITIES AND FLUORESCENCE OF A BACTERIAL PERIPLASMIC MALTOSE-BINDING PROTEIN, *Journal of Molecular Biology 214*, 337-352.
51. Shelburne, S. A., Fang, H., Okorafor, N., Sumby, P., Sitkiewicz, I., Keith, D., Patel, P., Austin, C., Graviss, E. A., Musser, J. M., and Chow, D. C. (2007) MalE of group A Streptococcus participates in the rapid transport of maltotriose and longer maltodextrins, *J. Bacteriol. 189*, 2610-2617.
52. Schafer, K., Magnusson, U., Scheffel, F., Schiefner, A., Sandgren, M. O. J., Diederichs, K., Welte, W., Hulsmann, A., Schneider, E., and Mowbray, S. L. (2004) X-ray structures of the maltose-maltodextrin-binding protein of the thermoacidophilic bacterium Alicyclobacillus acidocaldarius provide insight into acid stability of proteins, *Journal of Molecular Biology 335*, 261-274.

APPENDIX

APPENDIX INHIBITION OF MALTOSE UPTAKE

A.1 Introduction

The maltose transporter from Streptococcus pneumonia is crucial to survival of the organism in the human host. Therefore, inhibitors of maltose uptake could, in theory, would prevent infection (*51*). Based on the crystal structure of MalEFGK2, which reveals the mode of interaction between maltodextrins and the two maltose-binding sites in the transporter, we propose that modifications at the non-reducing end of a maltodextrin might allow binding to MBP but prevent binding to MalF in the membrane. A mutation in the MalF binding site (G380D) that prevented maltose binding resulted in uncoupling of ATP hydrolysis from maltose transport (*48*), and suggested that a similar modification of the sugar substrate might result in the consumption of ATP while inhibiting maltodextrin (nutrient) uptake, leading to the death of the bacteria. The *St. pneumonia* maltose transporter is a member of the ATP-binding cassette superfamily, bearing similarity to the *E. coli* maltose transporter. We plan to test our hypothesis in the better characterized maltose system before working with S. pneumonia.

In collaboration with the group of Dr. Alexander Wei at Purdue University, we designed and chemically synthesized a molecule, named gal-glu4. It consists of one lactose unit and one maltotriose unit (Figure 1). The reducing end of this drug mimics maltose and is supposed to bind with the maltose binding site of MBP (*52*). But unlike the alpha connection at the non-reducing end of maltose that binds the binding site at

MalFG, the non-reducing end of this drug has a beta connection that is expected to be unable to bind MalFG. Our lab has found (data not published) that gal-glu4, like maltose, can stimulate ATPase activity of the *E. coli* maltose transporter. We hypothesize that gal-glu4 binds MBP and stimulates but fails to be transported may preferentially be bound by MBP and keep consuming ATP. If this is the case, the bacteria will be killed. A question of interest is whether a non-transported sugar analogue will be more effective as an inhibitor of maltose transport than one that is transported, such as maltotriose.

One method for testing our hypothesis is to determine whether lower concentrations of gal-glu4 are able to compete effectively for binding. *In vitro* maltose uptake assay was also conducted to evaluate maltose uptake inhibition by the drug.

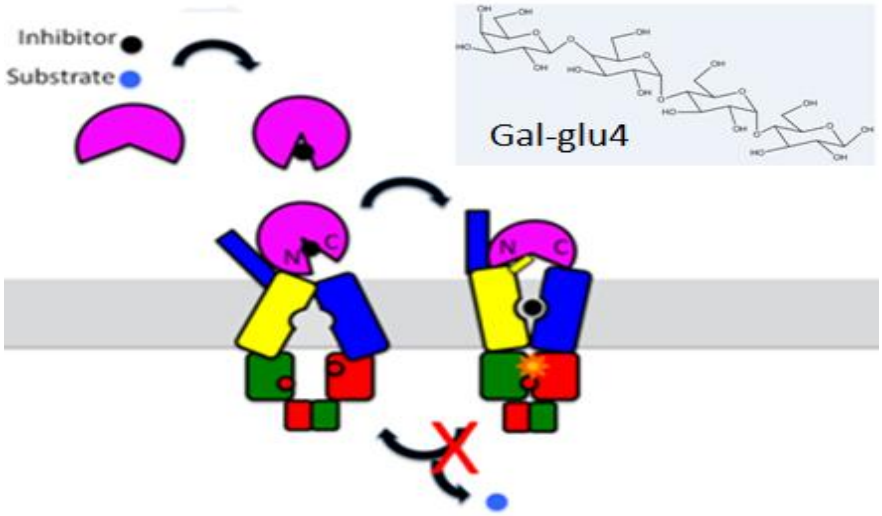

Figure A.1 The Model of Maltose Uptake Inhibition with Gal-glu4.

A.2 Methods

Preparation of proteoliposomes is needed to mimic the natural environment in which the maltose transporter complex is stabilized in membrane and the uptake of maltose is from outside to the inside of the lipid vesicle. Proteoliposomes are prepared following the description in (*33*).

H^3-Maltose Transport Assay. The ratio of lipid: $MalFGK_2$ in the proteoliposome was 100:1 (w/w). The protein concentration was determined to be about 0.80 mg/ml with an Amido Black assay. 35mM ATP and 20mM MgCl2 were added to the suspension buffer and the PLV was flash frozen with dry ice and slowly thawed in the ice-water bath 6 times and then sonicated 10s on/off for 3 times until it became transparent. For the transport assay, I used 2 μM 200 μCi/L H3-maltose. 25ul of the sample was loaded at each time point onto the filter which connected to a pump. The filters were rinsed, dried and then the radioactivity associated with the filters was read by a Liquid Scintillation Counter.

A.3 Results

Figure 2 shows the dissociation constant (Kd) of maltose is 2.11±0.22 μ M and the Kd of gal-glu4 is 2.13±0.22 μ M (3 μ M, ref 21). Their binding affinities are very close.

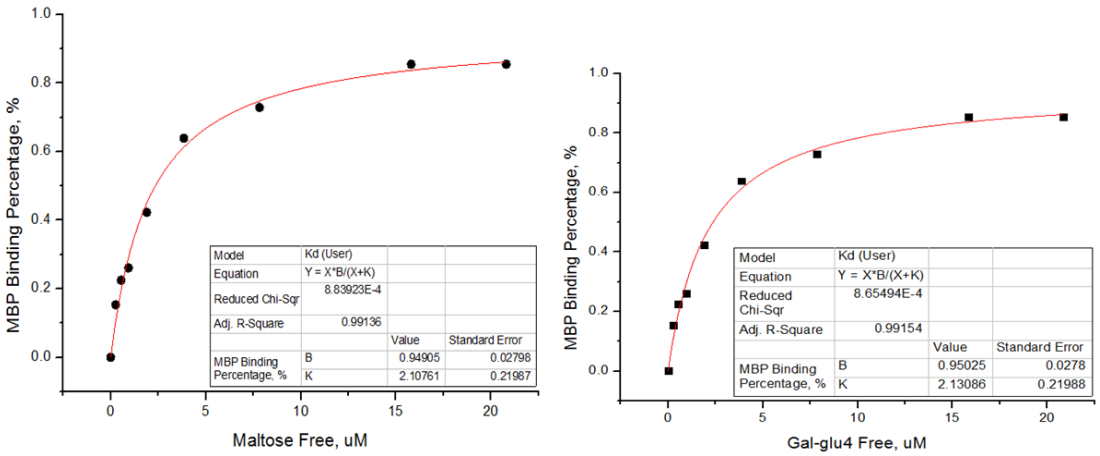

Figure A.2 Binding Curve and Binding Affinity of MBP with gal-glu4 (left) and maltose (right).

The result of the *in Vitro* Maltose Transport Assay with Proteoliposomes is shown in Figure 3. Maltose uptake is saturated within 30s when MBP is 1 or 2 μ M while the one of the 0.5 μ M MBP group continued to take up maltose for 70 seconds. The maltose uptake saturation amount appears similar for 0.5 to 2 μ M MBP. The result indicates that using lower amounts of MBP slows down the rate of maltose uptake while maintaining the maximum amount of maltose that can be taken up. Therefore, 0.5uM MBP is used for the uptake assays.

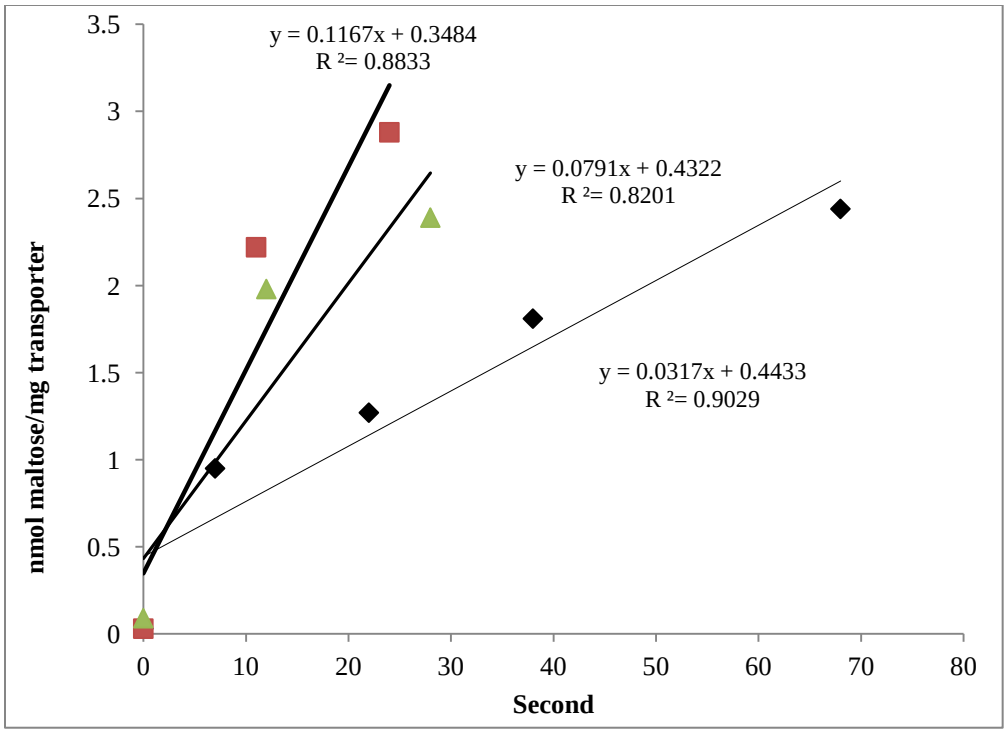

Figure A.3 Maltose Uptake Assay with 0.5 (blue), 1 (red), and 2 (green) μM MBP, and $MalFGK_2$ reconstituted in proteoliposomes.

The initial maltose uptake rates of the maltose transporter reconstituted in proteoliposomes are listed in Table 1. The initial uptake rates of the samples in the presence of gal-glu4 are lower than those without gal-glu4. However, the error of the duplicate uptake initial rates of maltose transporter in the presence of 2 μM maltose and 1 μM MBP is as large as about 10 fold (0.00898 versus 0.00097 nmol/mg/s). The assay was attempted to be reproduced and the results are shown in Table 2. But the errors between duplicates are still as large as 1.5 to 2 fold.

Table A.1 H^3-Maltose uptake assay initial rate in the presence of gal-glu4

	Initial Rate	R^2
2 μ M maltose, 0.5 μ M MBP	0.0162	0.9927
2 μ M maltose, 1 μ M MBP	0.0898	1
2 μ M maltose, 1 μ M MBP (Duplicate)	0.0097	0.7273
2 μ M maltose, 0.5 μ M MBP, 1 μ M gal-glu4	0.0079	0.9983
2 μ M maltose, 1 μ M MBP, 2 μ M gal-glu4	0.0078	0.9708

The unit of initial rate in the table is nmol/mg/s. The R^2 written as "1" was because only two data points are plotted before saturation in 30s.

Table A.2 H^3-Maltose uptake assay initial rate in the presence of gal-glu3, gal-glu4 or maltotriose

	Duplicate 1		Duplicate 2		Average Initial Rate
	Initial Rate	R^2	Initial Rate	R^2	
2 μ M maltose	0.031	1	0.0117	1	0.0214
2 μ M maltose + 1 μ M gal-glu4	0.0034	1	0.0046	0.9768	0.0040
2 μ M maltose + 2 μ M gal-glu4	0.0056	0.9071	0.0072	0.8593	0.0064
2 μ M maltose + 4 μ M gal-glu4	0.0036	0.8660	0.0067	0.9789	0.0052
2 μ M maltose + 20 μ M gal-glu3	0.0065	0.9788	ND	ND	0.0065
2 μ M maltotriose	0.0066	0.9582	ND	ND	0.0066
4 μ M maltotriose	0.0031	0.8373	ND	ND	0.0031

In this assay, 2uM ^{3}H maltose and 1uM MBP are present in each sample. The unit of the initial rate is nmol/mg/s. ND: not determined. The R^2 written as "1" was because only two data points are plotted before saturation in 30s.

A.4 Discussion

The reported K_d for maltotriose binding to MBP is 0.16 μM (*42*), much lower than that of maltose. Our results are consistent with this low dissociation constant by showing a bigger initial uptake rate in the presence of 2 μM maltotriose and 2 μM maltose than in the presence of 2 μM maltose alone. More experiments will be needed to determine the Ki for maltotriose.

In comparison of the row 2 and row 5 in Table 1, the maltose uptake initial rate in the presence of only 1 μM gal-glu4 is 10 times lower than that without gal-glu4. We would be excited if this result is reproducible. However, the errors between the duplicates undermine firm conclusions about the inhibition effectiveness of gal-glu4. Unfortunately, these drugs are unavailable to repeat these results.

VITA

VITA

Yan Huang was born on August 27, 1988, in Jinan, Shandong Province, China. Her grandpa, an excellent architect, impressed her by the passion and perseverance to science. Her grandma, a farmer and worker, taught her to work hard and love people generously. She was enrolled by Dept. of International Studies, Zhejiang University in 2006. The resource crisis and pollutions in China drove her to switch major from English to Environmental Science in 2008. She developed an interest in doing research during working in the Xu laboratory in her sophomore and junior years. The summer research experience in Dr. Karen McDonald's laboratory at UC Davis made her determined to studying biotechnology oversea. She fell in love with Hang Yu at Zhejiang University and keeps a long-distance relationship with him since then. She became a PhD candidate at Purdue University in December 2012. The sad news that her advisor, Dr. Amy L. Davidson died of cancer did not stop her from pursuing excellence, in the memory of such a great advisor and scientist. Now she is ready to face the new challenges of studying developmental biology in Dr. Umulis' group.